

bradscholars

Impact of pH on CuO/SnO₂ nanomaterials synthesis in electrochemical reduction of CO₂ to produce C₁/C₂ carboxylic acids

Item Type	Article
Authors	Al-Shamari, Mansoor;Khodary, A.;Zavahir, S.;Mujtaba, Iqbal;Han, D.S.;Rahmanian, Nejat
Citation	Al-Shamari M, Khodary A, Zavahir S et al (2025) Impact of pH on CuO/SnO ₂ nanomaterials synthesis in electrochemical reduction of CO ₂ to produce C ₁ /C ₂ carboxylic acids. Emergent Materials. 8: 4131-4150.
DOI	https://doi.org/10.1007/s42247-025-01037-4
Rights	(c) 2025 SpringerNature. This version of the article has been accepted for publication, after peer-review (when applicable) and is subject to Springer Nature's AM terms of use, but is not the Version of Record and does not reflect post-acceptance improvements, or any corrections. The Version of Record is available online at: https://doi.org/10.1007/s42247-025-01037-4 .
Download date	2026-05-18 03:59:27
Link to Item	https://bradscholars.brad.ac.uk/handle/10454/20324

Impact of pH on CuO/SnO₂ nanomaterials synthesis in electrochemical reduction of CO₂ to produce C1/C2 carboxylic acids

Mansoor Al-Shamari^{a,b,c*}, Ahmed Khodary^c, Fathima Sifani^b, Iqbal M Mujtaba^a, Dong Suk Han^b, and Nejat Rahmanian^{a*}

^a Chemical Engineering Program, Faculty of Engineering & Digital Technologies, University of Bradford, Bradford BD7 1DP, UK

^b The Center for Advanced Materials, Qatar University, Qatar.

^c Qatar Shell Research Technology Center (QSRTC), Qatar.

*Corresponding author m.k.m.al-shamari@bradford.ac.uk, and n.rahmanian@bradford.ac.uk,

Abstract

The electrochemical reduction of carbon dioxide into value-added chemicals is a promising solution to mitigate greenhouse gas emissions while producing sustainable fuels. In this study, CuO/SnO₂ nanomaterials (NM) were synthesized using the sol-gel technique under varying pH conditions in acidic and alkaline to investigate their impact on material properties and electrochemical performance for CO₂ reduction. The synthesized CuO/SnO₂ NM were characterized using XRD, TEM, SEM, XPS, and FTIR to analyze their morphology, crystallinity, and surface properties. Results revealed that CuO/SnO₂ NM prepared in alkaline media exhibited superior homogeneity, stability, and reduced particle size compared to acidic conditions, as confirmed by surface analysis. Electrochemical studies conducted in a two-compartment cell with a Ni foam cathode coated with CuO/SnO₂ (1:1) demonstrated higher activity and selectivity in alkaline-prepared NM. Specifically, the alkaline-synthesized nanomaterials achieved a Faradaic efficiency (FE) of 87% for the overall of formic acid and oxalic acid at -1.4 V in a 0.5 M KHCO₃ electrolyte, producing a maximum formic acid concentration of 1186 mg/L after 3 hours. In contrast, materials synthesized in acidic media displayed agglomeration and reduced stability, leading to lower FE and current efficiency. XPS analysis confirmed the partial reduction of Cu²⁺ to Cu⁺ in alkaline-prepared nanomaterials during CO₂ electrochemical reduction, highlighting their enhanced catalytic activity and stability. The study highlights the critical role of pH in controlling the morphology and electronic properties of CuO/SnO₂ nanomaterials synthesized via the sol-gel method. The enhanced CO₂ reduction performance in alkaline-prepared nanomaterials is attributed to their higher surface area, uniform distribution, and improved electron transfer characteristics. This work provides a cost-effective strategy for fabricating efficient electrocatalysts for CO₂ reduction, particularly targeting C1/C2 carboxylic acids production.

Keywords. CO₂ electroreduction; CuO/SnO₂ nanomaterials; sol-gel synthesis; electrocatalysis; Faradaic efficiency; C1/C2 carboxylic acid.

Abbreviations:

BE - Binding energy

CO₂ – Carbon dioxide

CO₂RR – Carbon dioxide reduction reaction

CuO/SnO₂ - Copper-Tin oxides.

DAC - direct air capture

eCO₂RP – Electrochemical CO₂ reduction Process

eCO₂RC – Electrochemical CO₂ reduction cell

ECR – Electrochemical reduction

FE – Faradaic efficiency

FTIR - Fourier-transform infrared spectroscopy

FWHM - Full width at half maximum.

GHG – Greenhouse gas

HCOOH- Formic acid, (FA)

CH₃COOH - Acetic acid.

CH₃OH- Methanol.

H₂C₂O₄ or (CO₂H)₂ Oxalic acid, (OA)

C₂H₅OH - Ethanol

IC- Ion chromatography

J - Current density (mA/cm²)

LiCl₂ - Lithium chloride

NM- Nanomaterials

NMP- N-methyl- pyrrolidone

PVDF - polyvinylidene fluoride

SnCl₂ - Tin chloride

s, p, d, f - the electron configuration for the electron's distribution of the atom

SEM - Scanning electron microscopy

TEM- Transmission electron microscopy,

XRD - X-ray diffraction

1. Introduction

The alarming increase in atmospheric carbon dioxide (CO₂) levels, driven primarily by human activities, is a major contributor to global climate change [1], [2], [3]. To address this issue, various strategies have been proposed and implemented to mitigate CO₂ emissions [4], [5]. These include carbon capture and storage (CCS) [6], which involves capturing CO₂ emissions at their source and storing them in geological formations, and direct DAC [7], a technology designed to remove CO₂ directly from the atmosphere. While these methods are effective in reducing atmospheric CO₂ concentrations, they are often energy-intensive and lack economic incentives due to their limited end-use applications. An alternative approach lies in nature-based solutions, such as reforestation, afforestation, and soil carbon sequestration [8], which enhance natural CO₂ absorption processes. These methods are cost-effective but limited by land availability and timescales required for significant impact. Another promising avenue is CO₂ utilization, which transforms captured CO₂ into valuable chemicals, fuels, and materials, offering both environmental and economic benefits. Among these, eCO₂R [9], [10], [11], [12]; [13] has gained considerable attention due to its ability to directly convert CO₂ into value-added products using renewable energy sources. The simplified schematic representation of the eCO₂ reduction process (eCO₂R) can be divided into three primary regions, as illustrated in Fig. 1. The first region is the electrode surface, where the eCO₂R occurs on the cathode. The efficiency and selectivity of these reactions are heavily influenced by the material type and surface structure of the cathode. The second region is the mass transport layer, often referred to as the "migration layer." This layer governs the transport of radical intermediates from the electrode surface to the electrolyte solution. It includes the diffusion layer, where molecular transport is driven by concentration gradients. Efficient mass transport is crucial for enhancing the reaction rate and preventing reversible reactions. The performance of this layer plays a vital role in the overall efficiency of the electrochemical cell and the selective extraction of specific products. The final region is the bulk solution, which constitutes the larger volume of electrolyte surrounding the electrode and the mass transport layer. This solution serves as a reservoir for CO₂ and other reactants while also absorbing heat generated during the electrochemical reactions. The composition of the bulk solution, including its pH and ionic strength, significantly influences the reaction dynamics. A well-designed electrolyte ensures efficient CO₂ reduction at the electrode surface while maintaining a continuous supply of reactants and enabling the effective removal of products. This three-region framework highlights the interplay of electrode surface properties, mass transport, and electrolyte composition in determining the efficiency and selectivity of the eCO₂R process [19].

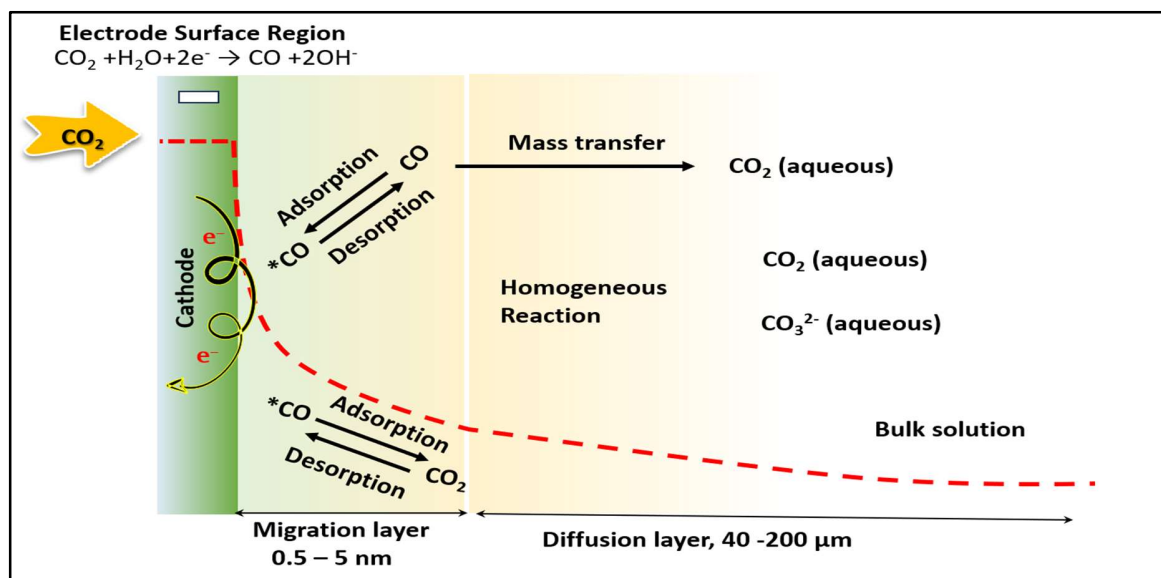


Fig. 1. A schematic description eCO₂RP composed of electrode surface region, mass transport layer and bulk solution [19].

This technology not only mitigates CO₂ emissions but also contributes to the circular carbon economy by producing commercially viable products [14], [15]. eCO₂R enables the selective production of chemicals such as formic acid, oxalic acid, carbon monoxide, methane, and ethanol, which are essential in various industrial applications [16], [17]. Formic acid and oxalic acid, in particular, are attractive due to their roles as chemical feedstocks and their potential for use in energy storage systems [18], [19]. The efficiency of this process, however, hinges on the development of advanced electrocatalysts that can drive the multi-electron and proton-coupled reactions required for CO₂ conversion with high activity, selectivity, and stability. Copper-based catalysts are well-known for their versatility in facilitating multi-electron transfer reactions, enabling the production of a wide range of CO₂ reduction products [20], [21], [22], [23]. SnO₂ on the other hand, is recognized for its excellent ability to stabilize reaction intermediates and facilitate selective proton-coupled electron transfer [24], [25], [26]. Combining these materials into CuO/SnO₂ nanostructures leverages the strengths of both components, creating a synergistic effect that enhances catalytic activity, selectivity, and stability [27], [28]. While several studies have explored CuO and SnO₂ independently, the combined effect of CuO/SnO₂ as a composite electrocatalyst remains underexplored, particularly in the context of tailoring synthesis conditions to optimize performance [29], [30]. The synthesis method plays a pivotal role in determining the structural, electronic, and surface properties of the catalyst. Among various approaches, the sol-gel method stands out due to its simplicity, scalability, and ability to produce highly homogeneous

nanostructures with controlled compositions. However, the influence of synthesis parameters, such as pH, on the catalytic performance of CuO/SnO₂ nanomaterials has not been systematically investigated. pH variations during synthesis can significantly alter the crystallinity, particle size, surface area, and electronic properties of the resulting materials, ultimately affecting their performance in eCO₂R [27], [28].

This study focuses on the pH-controlled sol-gel synthesis of CuO/SnO₂ (1:1) nanomaterials and evaluates their catalytic activity for CO₂ reduction. The novelty of this work lies in three critical aspects: (i) Impact of synthesis pH on material properties: This study uniquely compares CuO/SnO₂ nanomaterials synthesized under acidic and alkaline conditions. Detailed characterization using SEM, TEM, XRD, XPS, and FTIR highlights significant differences in particle size, homogeneity, crystallinity, and stability, directly correlating these properties to the pH conditions during synthesis, (ii) Enhanced selectivity and stability: to demonstrate that CuO/SnO₂ nanomaterials prepared in alkaline media exhibit superior catalytic performance, achieving a high value at -1.4 V in a 0.5 M KHCO₃ electrolyte. This result surpasses many existing catalysts in terms of cost-effectiveness and efficiency [31], [32]. The alkaline-prepared materials also show enhanced stability during prolonged electrochemical operation, and (iii) Cost-Effective and scalable approach: By utilizing a conventional sol-gel method, this work provides a low-cost and scalable strategy for producing stable CuO/SnO₂ catalysts, making it suitable for industrial applications. The findings not only offer new insights into the role of synthesis pH in catalyst design but also highlight the practical potential of CuO/SnO₂ nanomaterials for sustainable CO₂ electroreduction. By comparing materials synthesized under acidic and alkaline conditions, we investigate how pH influences their structural properties and performance in producing formic acid (C1 product) and oxalic acid (C2 product). Detailed characterization using XRD, SEM, TEM, XPS, and FTIR reveals critical insights into the relationship between synthesis conditions and catalyst functionality. Electrochemical studies highlight the superior activity, selectivity, and stability of alkaline-prepared CuO/SnO₂ nanomaterials. This work provides a comprehensive understanding of how synthesis parameters affect the catalytic performance of CuO/SnO₂ nanomaterials, emphasizing the role of pH in tailoring active sites and reaction pathways. The findings pave the way for designing cost-effective, scalable, and high-performance electrocatalysts for sustainable CO₂ conversion.

2. Materials and methods

2.1. Preparation of Nanomaterials (NM) by the wet method:

NM has been synthesized in acidic and alkaline media to produce different morphologies, structures, and metal distributions of 1:1 mass ratio composition of CuO/SnO₂ nanocomposite. CuO/SnO₂ (1:1) NM has been prepared and developed by the sol-gel method and to coat cathode electrode. To run different experiments at different operation conditions.

2.1.1. Chemical and materials

The following chemicals and materials were used to prepared CuO/SnO₂ form different sources is shown as follows: SnCl₂.2H₂O (98%), Cu(CH₃COO)₂ (98%), Polyvinylidene PVDF and NMP were purchased from Sigma Aldrich, Polyethylene glycol was purchased from BDH, NaOH granulated was purchased from EMPLURA, and Acetylene carbon was purchased from MTI company. The ultra-pure deionized water was produced from the Millipore Mille-Q system.

2.1.2. Preparation of CuO/SnO₂ (1:1) NM:

Equal mass ratio of CuO/SnO₂ nanocomposite has been prepared and developed by the sol-gel method to use as catalytic material and coated cathode electrode. The first batch (alkaline matrix) for 1:1 composition of CuO/SnO₂ nanocomposite was prepared at pH 10 by mixing copper acetate and Tin chloride solutions with 10M NaOH as a precipitating agent. The initial stage was to dissolve SnCl₂.2H₂O and Cu (CH₃COO)₂ individually dissolved in 40 ml absolute ethanol to form a 0.1M solution and agitated for one day. The two solutions were blended, and 4 ml of polyethylene glycol was used as a precursor. Again, a few dropwise of 10M NaOH were added to adjust the pH at 10. The obtained solution has been mixed intensively for one day followed by washing with ethanol several times for the removal of the impurities and easy drying of the composite. The precipitate thus received has been dried at 80 degrees using a hot air oven followed by the calcination at 500 degrees for 2 hrs. [33]. The second batch (acid matrix) for 1:1 composition of CuO/SnO₂ nanocomposite was Prepared at pH 5.5 by dissolving CuCl₂.2H₂O in 20 ml deionized water and 1 ml 3M HCl. SnCl₂.2H₂O was added to the solution and mixed well to form a clear solution. Consequently, in a 100 ml beaker, the solution was gently added to 10 ml of fresh 10 mM NaBH₄ solution and mixing well, abundant black precipitates were observed during mixing. Continuous stirring was made until precipitates aggregates together and the supernatant is Color-less. The product was filtered several times with deionized water to eliminate unreacted precursors, and using vacuum filtration to collect the products, and overnight dried under vacuum and followed by calcination at 500 °C for 2 hrs. [34].

2.1.3. Coating of cathodic electrode

80 mg of the synthetic nanomaterial were combined with 10 mg of PVDF and 10 mg of acetyl carbon, then thoroughly pulverized in a mortar. The mixture was then put into a tiny glass vial, 600 μl of NMP was added, and the mixture was sonicated for at least one hour to improve nanoparticle dispersion. then, the finished mixture was coated on a third of a nickel foam (4x2 cm) and allowed to dry at 60 °C.

2.2. Chemical analysis:

HCOOH, and H₂C₂O₄ have been analyzed by ion chromatography (IC) (Metrohm 930) equipped with a separation column AS14 (4 ×250 mm) as stationary phase, the flow rate of the mobile phase is 1 mL/min of 0.5 mM of H₂SO₄ and 0.1M LiCl₂ used for regenerator and suppressor [19]. pH and electrical conductivity (E.C) have been performed using a HACH model HC201 pH-meter and HQD portable Conductivity meter respectively.

2.3. Surface Characterization of NM

Structural characteristics of CuO/SnO₂ nanocomposites were determined using X-ray diffraction patterns were analyzed with an X-ray Diffractometer (PANalytical) with Cu-K α radiation ($\lambda = 1.5417 \text{ \AA}$) with 40 KV and 30 mA in 10 to 90°. FTIR measurements were performed on Perkin Elmer instrument in 600 to 4000 cm^{-1} range with 32 scans, SEM images were collected in ThermoScientific Quanta 650 with Qantas 400 EDS instrument, TEM images were collected in ThermoScientific TALOS 650 with Qantas 400 EDS instrument and XPS measurements were performed on ThermoScientific ESCALAB 250i.

2.4. Electrochemical measurements:

As shown in Fig. 2, the eCO₂R cell was constructed by using the one-compartment cell system used to run different experiment in aqueous electrolytic solutions of KHCO₃ and K₂SO₄ using Pt, SnO₂-CuO material coated Ni foam as counter and working electrode respectively, and saturated calomel electrode (SCE) as reference electrode. Cyclic voltammetry (CV) experiments were carried out using a Gamry instrument 1010 and all CV measurements were performed at room temperature. The experiments were taken up by deaerating the electrolyte by purging N₂ gas to eliminate any oxygen may be exist for 10 min followed by CO₂ saturation of the electrolyte for 30 min. Potentiostatic tests were conducted under a constant potential value for the desired time. Several experiments have been done to optimize the operating conditions at different voltages from -0.5 to -1.4V, reaction time, saturated electrolyte solution KHCO₃, K₂SO₄ and CuO/SnO₂ nanomaterials prepared by sol-gel method in acid and alkaline media.

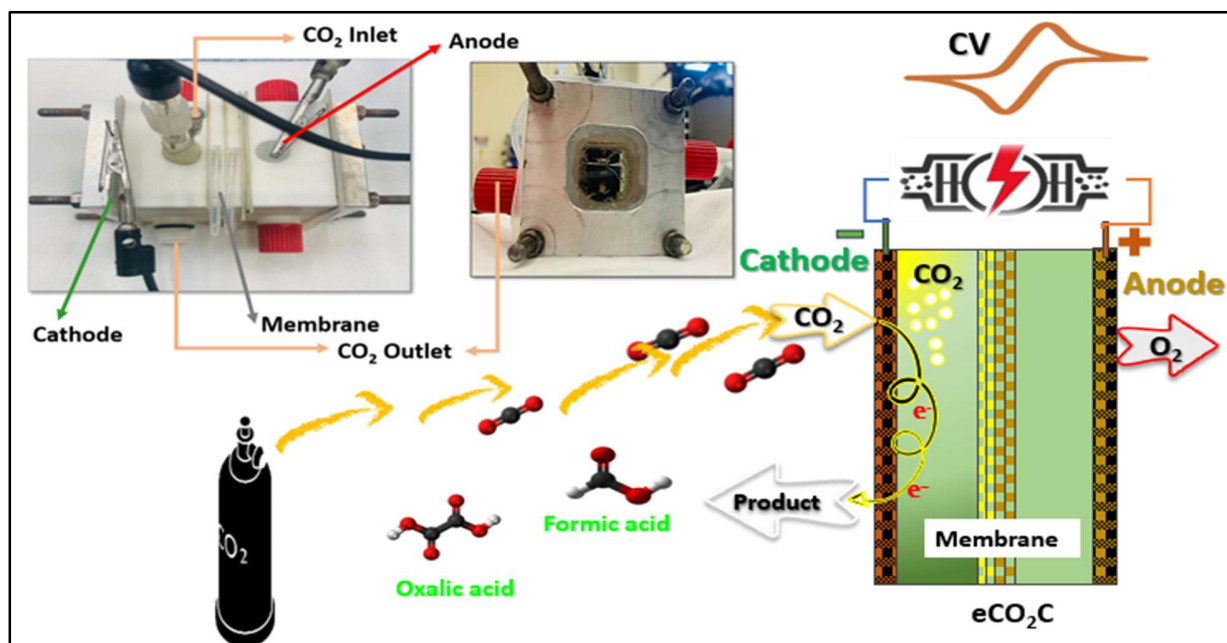


Fig. 2. Electrochemical setup used during eCO₂R experiments in cyclic voltammetry and potentiostatic electrolysis.

3. Results and Discussion

3.1. Structural Characterization

3.1.1. FTIR Analysis of CuO/SnO₂ Nanomaterials: FTIR spectroscopy was employed to identify the functional groups and bonding interactions in CuO/SnO₂ nanomaterials synthesized under acidic and alkaline conditions. Fig. 3 presents the FTIR spectra of fresh CuO/SnO₂ (1:1) NM samples prepared by sol-gel method in alkaline medium, and acid medium. For fresh nanomaterials, distinct peaks were observed in both acidic- and alkaline-prepared samples. In the alkaline-prepared CuO/SnO₂, the broad absorption band at ~3420 cm⁻¹ corresponds to O–H stretching vibrations from surface hydroxyl groups or adsorbed water molecules. The peak intensity was higher for alkaline-prepared samples, indicating a greater surface hydroxylation, which is known to enhance catalytic activity by facilitating CO₂ adsorption and activation. Similarly, a weaker O–H band was observed in acidic-prepared samples, reflecting a lower degree of surface hydroxylation. In both samples, a strong and sharp band at ~520–530 cm⁻¹ corresponds to the Cu–O stretching vibrations, confirming the presence of CuO in the nanomaterials [35], [36]. The Sn–O stretching vibrations were identified at ~ 600–620 cm⁻¹, which are characteristic of SnO₂. In alkaline-prepared samples [35], [36], these bands were sharper and more distinct compared to the acidic-prepared samples, suggesting better-defined CuO and SnO₂ phases with

fewer structural defects. Additional peaks at $\sim 1400\text{--}1500\text{ cm}^{-1}$ were attributed to carbonate species (CO_3^{2-}), possibly due to atmospheric CO_2 adsorption during the synthesis and drying processes [35], [36]. The intensity of these peaks was slightly higher in alkaline-prepared samples, indicating a greater tendency for CO_2 -related interactions. The FTIR analysis underscores the importance of synthesis pH in determining the structural and surface properties of CuO/SnO_2 nanomaterials.

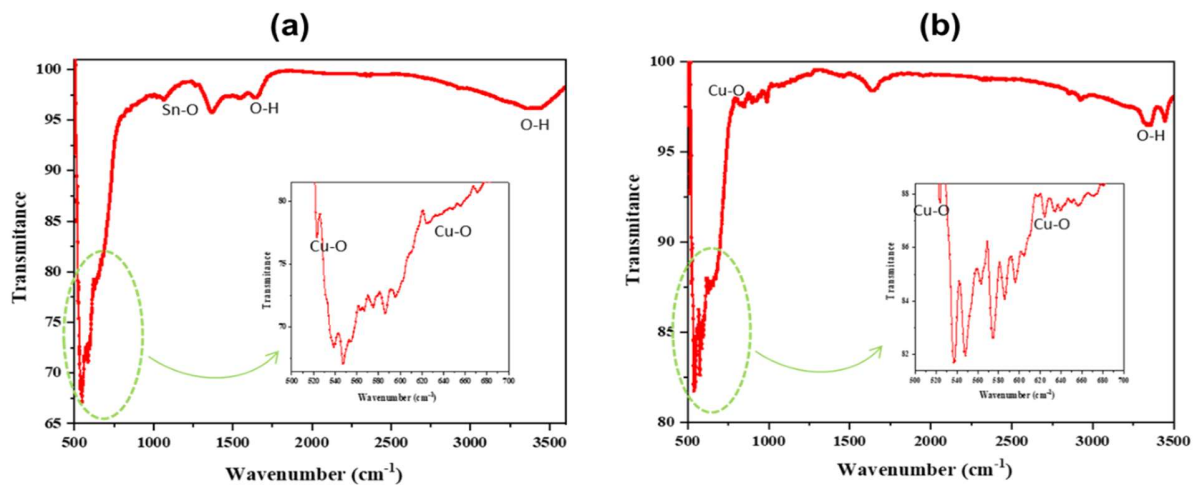


Fig. 3. FTIR spectra of fresh CuO/SnO_2 (1:1) NM samples prepared by sol-gel method in **a)** alkaline medium, and **b)** acid medium.

3.1.2. XRD Analysis of CuO/SnO_2 Nanomaterials

The crystal structure and phase composition of the CuO/SnO_2 nanomaterials (NM) synthesized under acidic and alkaline conditions were analyzed using X-ray diffraction (XRD). The XRD patterns were obtained for fresh nanomaterials and compared to identify the influence of pH on the crystallinity, phase purity, and structural properties of the materials (see Fig. 4). For the nanomaterials prepared in alkaline media, the XRD patterns revealed well-defined and sharp peaks, indicative of high crystallinity. The diffraction peaks corresponding to CuO were identified at $2\theta = 35.5^\circ$ (111), 38.7° (200), 48.9° (202), and 61.5° (220), which match the monoclinic phase of CuO (JCPDS 05-0661). Similarly, peaks corresponding to the tetragonal SnO_2 phase were observed at $2\theta = 26.6^\circ$ (110), 33.8° (101), and 51.6° (211), consistent with the reference pattern (JCPDS 41-1445). The higher intensity and sharpness of these peaks in the alkaline-synthesized samples indicate a more crystalline structure with well-ordered CuO and SnO_2 phases. The relative intensity of the CuO peaks was slightly enhanced, suggesting a larger crystallite size and better phase development under alkaline conditions. In contrast, the nanomaterials synthesized in acidic media exhibited broader and less intense peaks, indicating lower crystallinity and the

presence of structural imperfections. The same characteristic peaks for CuO and SnO₂ phases were observed; however, the reduced intensity and peak broadening suggest smaller crystallite sizes and poorer phase formation. Additionally, the peak at $2\theta \approx 26.6^\circ$ for SnO₂ (110) was dominant, suggesting a relatively higher concentration of SnO₂ compared to CuO. This difference can be attributed to the slower nucleation and growth rates of CuO in acidic media, which may hinder its structural development. The crystallite size was calculated using the Scherrer equation [37],

$$D = \frac{K\lambda}{\beta \cos\theta}$$

where D is the crystallite size, K is the shape factor (0.9), λ is the wavelength of the X-rays (0.154 nm), β is the full width at half maximum (FWHM) in radians, and θ is the Bragg diffraction angle. For the alkaline-synthesized samples, the average crystallite size was found to be 18–22 nm, whereas for acidic-synthesized samples, it was smaller, ranging between 10–14 nm. This variation further confirms the influence of pH on the structural properties, where the alkaline medium promotes better crystallization and larger grain size [38], [39].

The XRD analysis clearly demonstrates that the synthesis pH significantly influences the crystallinity, phase composition, and crystallite size of the CuO/SnO₂ nanomaterials. The alkaline-prepared samples exhibited superior crystallinity and well-formed CuO and SnO₂ phases, which contribute to their enhanced stability and catalytic performance in electrochemical CO₂ reduction. In contrast, acidic-prepared samples showed smaller crystallite sizes and less developed phases, which are likely to impact their efficiency and long-term stability.

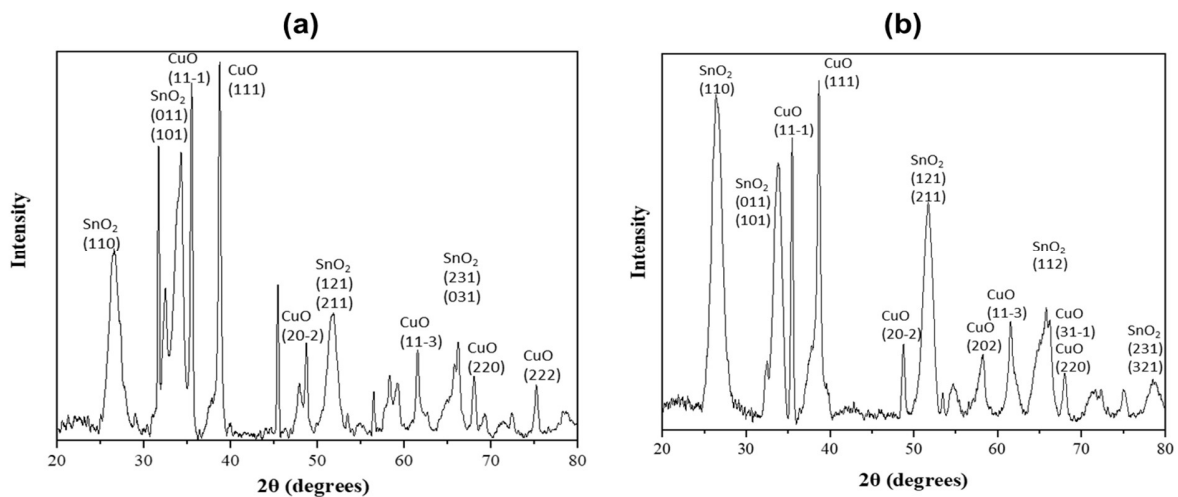


Fig. 4. XRD patterns of CuO/SnO₂ (1:1) NM samples prepared by sol-gel method in alkaline medium, and **b)** acid medium.

3.1.3. SEM, SEM-EDS, and TEM Analysis of CuO/SnO₂ Nanomaterials

SEM was employed to analyze the surface morphology and particle distribution of CuO/SnO₂ nanomaterials synthesized under acidic and alkaline conditions. For the alkaline-prepared samples, the SEM images revealed uniformly distributed nanoparticles with minimal agglomeration (Fig. 5.a). The particles exhibited a spherical morphology with an average size range of 20–40 nm, contributing to a higher surface area and enhanced catalytic activity.

In contrast, acidic-prepared samples displayed irregularly shaped particles with significant agglomeration (Fig. 5.b). The particle size ranged between 50–100 nm, with larger clusters forming due to uneven nucleation and growth during the synthesis process. The poor distribution and larger particle size are likely to reduce the number of active sites available for CO₂ adsorption and reduction, impacting the overall catalytic performance [40].

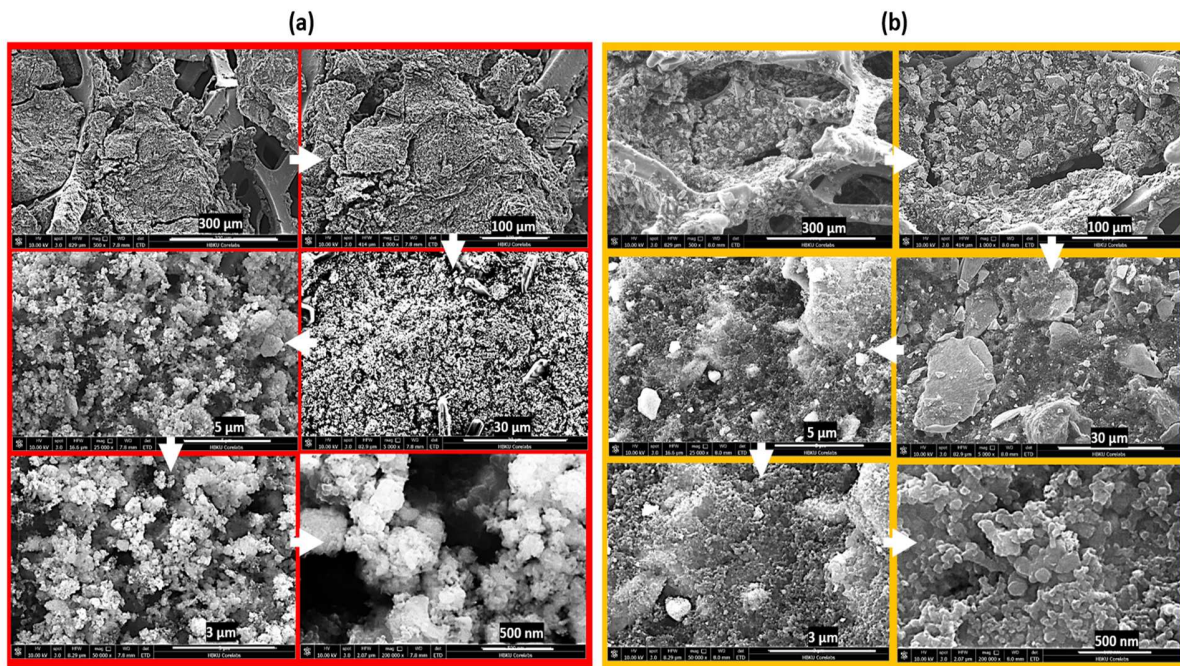


Fig. 5. Surface characterization by SEM within micro/nano scales for fresh sample of CuO/SnO₂ (1:1) NM prepared by sol-gel method in **a)** alkaline medium, and **b)** acid medium.

EDS integrated with SEM was performed to determine the elemental composition and distribution of Cu, Sn, and O in the nanomaterials (see Table 1). The EDS spectra of alkaline-prepared samples showed a uniform distribution of Cu and Sn elements, with a Cu/Sn atomic ratio close to the target 1:1. This uniformity indicates successful incorporation of both components during the sol-gel synthesis process. For acidic-prepared samples, the EDS analysis revealed a less homogeneous distribution of Cu and Sn, with localized enrichment of Sn regions. This

inhomogeneity could result from incomplete mixing or differential precipitation during the synthesis. Elemental mapping further highlighted the superior distribution of Cu and Sn in alkaline-prepared samples compared to acidic-prepared ones. The presence of oxygen in all samples was consistent with the formation of CuO and SnO₂ phases. However, the alkaline-prepared samples exhibited a higher density of surface oxygen, likely related to surface hydroxyl groups, which play a key role in CO₂ activation [39].

Transmission Electron Microscopy (TEM) was utilized to investigate the detailed structural features and particle size distributions of the CuO/SnO₂ nanomaterials. TEM images of alkaline-prepared samples revealed discrete nanoparticles with well-defined boundaries and average sizes ranging from 10–20 nm, corroborating the SEM results (see Fig. 6.a). The high-resolution TEM (HRTEM) images showed clear lattice fringes, with interplanar spacings of 0.231 nm and 0.335 nm, corresponding to the (111) plane of CuO and the (110) plane of SnO₂, respectively.

Table 1. SEM/EDS semi-quantitative element analysis of fresh CuO/SnO₂ samples prepared by sol-gel method in alkaline and acid.

Elements	Alkaline medium		Acidic medium	
	Elements at 40 μm (Atom %)	Elements at 2 μm (Atom %)	Elements at 40 μm (Atom %)	Element analysis at 2 μm (Atom %)
C	43.46	57.18	67.24	85.84
O	39.36	29.44	16.14	7.06
F	4.55	4.38	12.82	4.27
Al	0.40	0.07	0.06	0.04
Ni	0.22	0.18	1.13	0.13
Cu	2.66	4.25	0.16	0.06
Sn	2.95	4.33	3.09	2.57

These results confirm the formation of crystalline CuO and SnO₂ phases in alkaline-prepared samples. Acidic-prepared samples, in comparison, displayed larger and less defined nanoparticles, with sizes ranging from 30–50 nm (see Fig. 6.b). The HRTEM images showed fewer distinct lattice fringes, indicating reduced crystallinity. The electron diffraction patterns and TEM/EDS elemental analysis (Table 2) further supported these observations, with sharp diffraction rings in alkaline-prepared samples and broader, less distinct rings in acidic-prepared samples [41], [39].

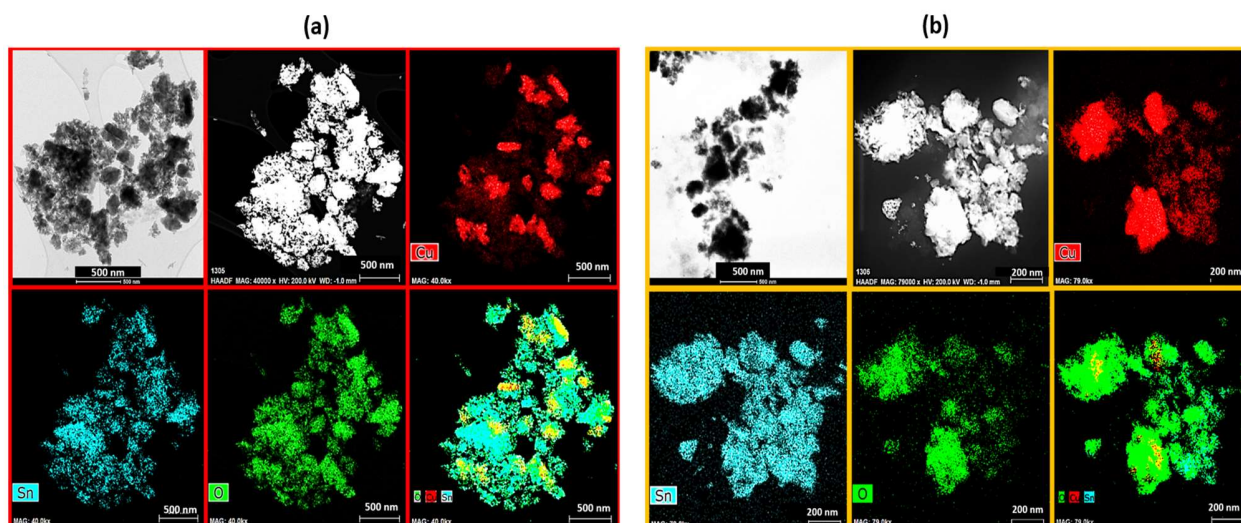


Fig. 6. TEM images of fresh sample CuO/SnO₂ (1:1) NM prepared by sol-gel method in **a)** alkaline medium, and **b)** acid medium.

Table 2. TEM/EDS elemental of fresh CuO/SnO₂ samples prepared by sol-gel method in alkaline and acid.

Elements	Alkaline medium (%)	Acid medium (%)
C	48.14	92.57
O	28.60	2.86
Cu	10.16	0.92
Sn	12.17	0.95
F	0.04	0.20
S	0.55	0.10
Si	0.22	2.17
Al	0.11	0.16

3.1.4. XPS Analysis CuO/SnO₂ Nanomaterials

X-ray photoelectron spectroscopy (XPS) was performed to investigate the surface composition, oxidation states, and chemical transformations of the CuO/SnO₂ nanomaterials (NM) synthesized in both acidic and alkaline media, before their use in electrochemical CO₂ reduction (eCO₂R). The analysis primarily focused on the Cu 2p, Sn 3d, O 1s, and C 1s spectra to identify changes in surface chemistry and assess material stability under operating conditions (Fig. 7 and 8). For fresh nanomaterials synthesized under alkaline conditions, the Cu 2p spectrum showed peaks at 933.9 eV for Cu 2p_{3/2}, along with a distinct satellite feature around 941 eV, confirming the presence of Cu²⁺ in the CuO phase (Fig. 7.a) [42]. The Sn 3d spectrum displayed two clear peaks at 486.8 eV for Sn 3d_{5/2} and 495.3 eV for Sn 3d_{3/2}, indicating the presence of Sn⁴⁺ in SnO₂ (Fig. 7.b) [43]. The O 1s spectrum revealed a primary peak at 531.0 eV corresponding to lattice

oxygen (O^{2-}) within the metal oxides, accompanied by a shoulder peak attributed to adsorbed hydroxyl species (Fig. 8.a) [44]. The C 1s spectrum exhibited peaks for C–C (sp^2/sp^3), C–O, and minor contributions from carbonate species, which were likely due to environmental contamination during sample handling (Fig. 8.c) [45]. In comparison, acidic-synthesized samples exhibited similar spectral features, although the Cu 2p peaks appeared broader and less intense, suggesting weaker CuO crystallinity and reduced structural homogeneity (Fig. 7.c). The Sn 3d peaks were consistent but showed minor shifts, implying a less uniform SnO_2 distribution (Fig. 7.c). The O 1s and C 1s spectra for acidic samples revealed higher proportions of adsorbed species, indicating increased surface reactivity and reduced material stability ((Fig. 8.c-d). The XPS analysis clearly demonstrates that CuO/ SnO_2 nanomaterials synthesized under alkaline conditions exhibit superior stability and structural integrity. In contrast, the acidic-prepared samples show evidence of degradation and reduced performance, characterized by the loss of CuO species and instability in the SnO_2 phase [46].

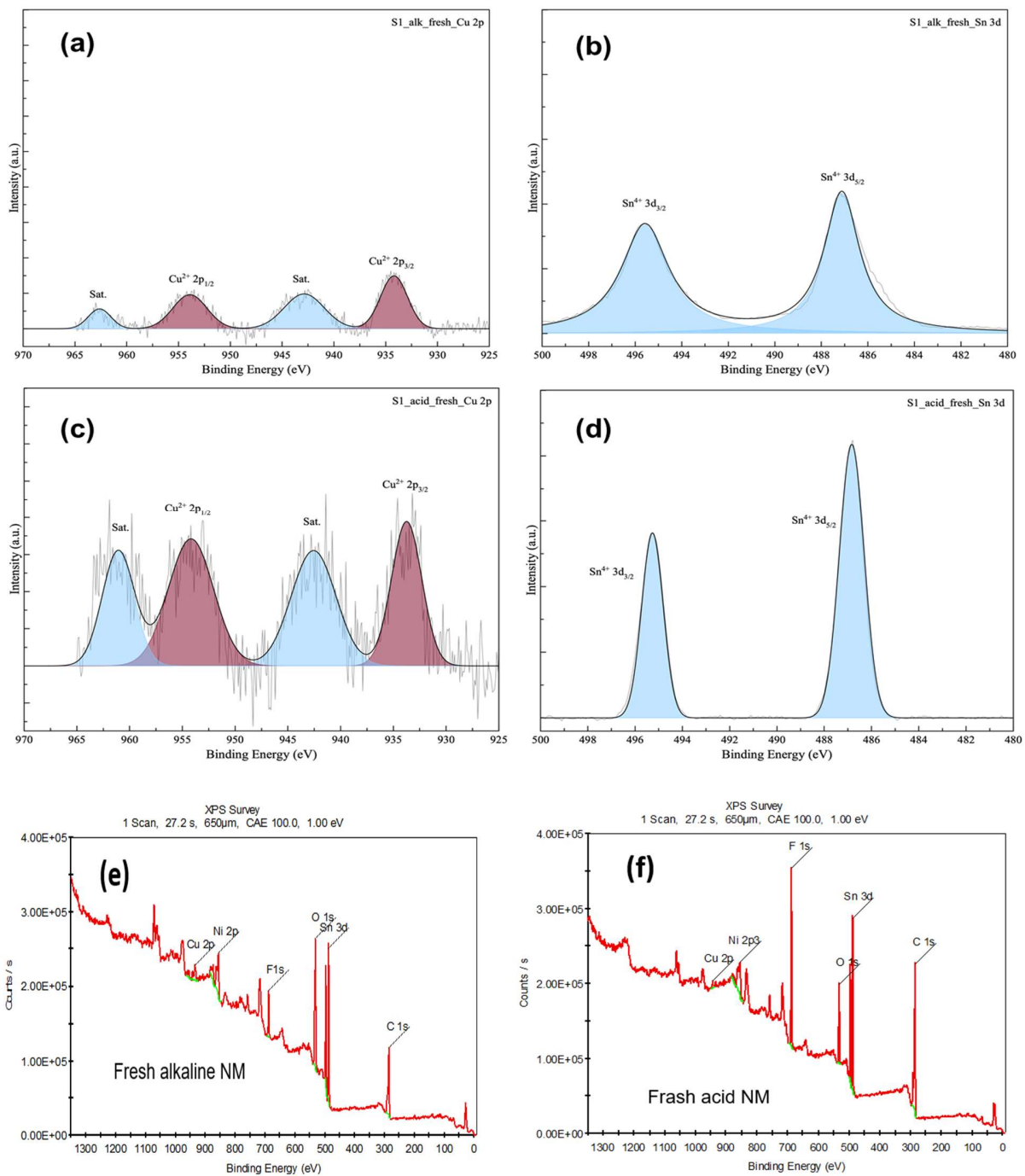


Fig. 7: XPS spectra of Cu 2p (a, c) and Sn 3d (b, d) of fresh CuO/SnO₂ NM samples prepared by sol-gel method in (a, b) alkaline medium, and (c, d) acid medium, (e, f) the XPS Survey spectrum taken with a pass energy of 100eV and step size of 1eV for fresh alkaline and acid sample.

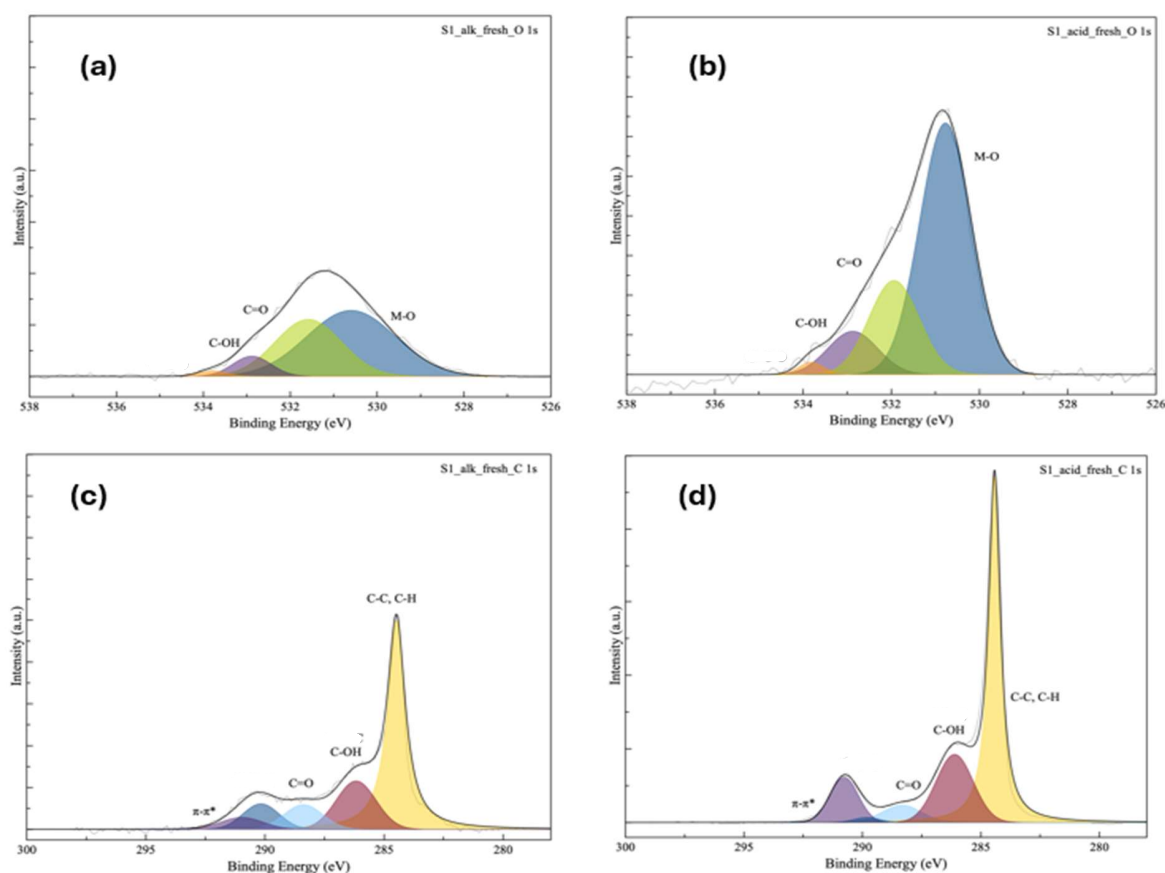


Fig. 8. XPS spectra of O 1s (a, c) and C 1s (b, d) of fresh CuO/SnO₂ NM samples prepared by sol-gel method in (a, c) alkaline medium, and (b, d) acid medium.

3.2. Electrochemical Analysis

The electrocatalytic performance of CuO/SnO₂ NM synthesized under acidic and alkaline conditions was thoroughly evaluated for CO₂ reduction in a two-compartment electrochemical cell. The cathode was prepared by coating Ni foam with CuO/SnO₂ nanomaterials (1:1), while the anode consisted of a Pt electrode. A 0.5 M KHCO₃ solution served as the electrolyte, saturated with CO₂ to create a favorable environment for the electrochemical reduction reaction. The configuration is described in Fig.1. Key performance metrics such as Faradaic efficiency (FE), current density (J), product selectivity, and catalyst stability were systematically analyzed.

3.2.1. Cyclic Voltammetry (CV) Studies

Cyclic voltammetry was employed to investigate the redox behavior of the CuO/SnO₂ electrodes in both N₂- and CO₂-saturated KHCO₃ electrolyte. Under N₂ saturation, the CV curves exhibited characteristic peaks corresponding to Cu²⁺/Cu⁺ and Sn⁴⁺/Sn²⁺ redox transitions, confirming the active participation of both components in electron transfer processes (Fig. 9). When saturated

with CO₂, a significant increase in current density was observed in the cathodic region, indicating the onset of CO₂ reduction. The alkaline-prepared nanomaterials displayed sharper and more pronounced reduction peaks compared to acidic-prepared samples, suggesting superior catalytic activity. The observed shift in peak potentials toward more positive values for the alkaline samples indicates reduced activation energy and improved charge transfer kinetics. Acidic-prepared samples, on the other hand, showed broader and less distinct peaks, suggesting lower efficiency and possible involvement of side reactions.

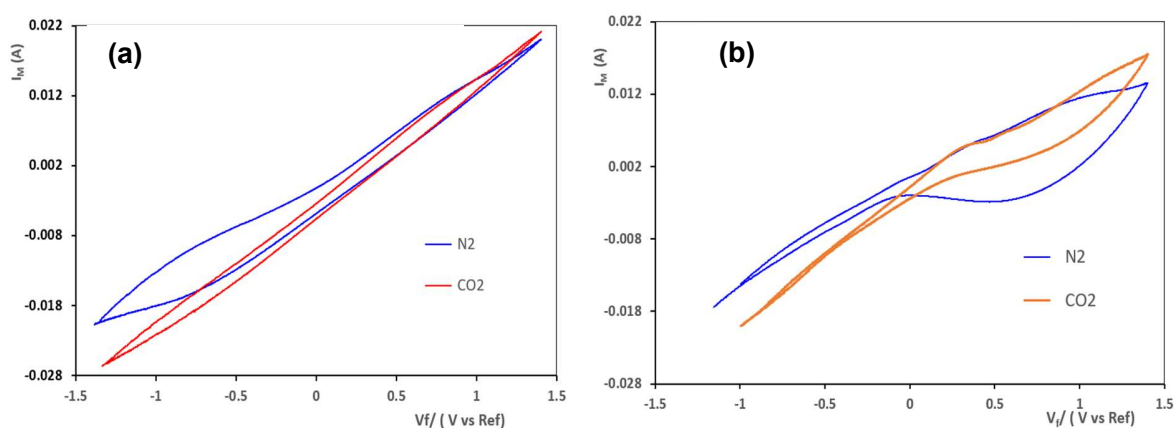


Fig. 9. CV graphs of Ni cathode coated with CuO/SnO₂ (1:1) NM prepared by sol-gel method in **a)** alkaline medium, and **b)** acidic medium by continuous purging of N₂ and CO₂. Electrolyte: 0.5 M KHCO₃, Anode: Pt, reference electrode: SCE, at a scan rate of 10 mV/s.

The enhanced current densities observed for alkaline samples are linked to their larger electrochemically active surface area, as inferred from electrochemical surface area (ECSA) measurements. The Tafel slopes were derived to assess the reaction kinetics. Alkaline-prepared samples showed a lower Tafel slope (~130 mV/dec) compared to acidic-prepared samples (~165 mV/dec), indicating faster kinetics and improved catalytic efficiency for CO₂ reduction.

3.2.2. Potentiostatic electrolysis and product analysis

Fig. 10 compares the FE of formic acid (FA), oxalic acid (OA), and the combined C1/C2 products for CuO/SnO₂ electrocatalysts synthesized in acidic and alkaline media. The FE for formic acid of alkaline prepared electrocatalyst is low, around 10-15%, indicating moderate selectivity for C1 products. The FE for formic acid of acid-prepared electrocatalyst is even lower, remaining below 10%, reflecting limited efficiency in producing formic acid in acidic-prepared electrocatalysts. The alkaline-prepared electrocatalyst shows slightly better selectivity for formic acid compared to the acidic-prepared electrocatalyst, possibly due to the superior surface properties and stability

observed in alkaline-prepared nanomaterials. The FE for oxalic acid of alkaline prepared electrocatalyst is significantly higher, reaching nearly 80%, demonstrating a strong preference for C2 product formation. The FE for oxalic acid of the acid-prepared electrocatalyst is much lower, approximately 20%, indicating that acidic-prepared electrocatalysts are less effective in generating C2 products. The stark difference between the two electrocatalysts highlights the enhanced electrocatalytic activity and structural stability of alkaline-prepared nanomaterials, which are more effective in promoting the formation of C2 products like oxalic acid. The total FE for C1/C2 products of alkaline prepared electrocatalyst approaches 90%, showcasing excellent efficiency in CO₂ electrochemical reduction across both product categories. The total FE of acid-prepared electrocatalyst is significantly lower, at approximately 30%, reflecting the overall reduced activity and selectivity of acidic-prepared catalysts. The alkaline-prepared electrocatalysts achieve far superior overall efficiency for CO₂ reduction, emphasizing their suitability for practical applications. Alkaline-prepared electrocatalysts dominate in performance across all metrics, particularly for oxalic acid (C2 product) formation and total C1/C2 efficiency. Acid-prepared electrocatalysts show significantly lower performance, likely due to poorer structural integrity, increased particle agglomeration, and reduced crystallinity observed in acidic-prepared nanomaterials. The results emphasize the importance of synthesis pH in optimizing catalytic properties, with alkaline conditions leading to enhanced product selectivity, stability, and overall efficiency. The data confirms that CuO/SnO₂ nanomaterials prepared in an alkaline medium are far superior for CO₂ reduction, achieving higher Faradaic efficiencies for both C1 and C2 products. These findings highlight the potential of alkaline-prepared electrocatalysts for practical and scalable CO₂ reduction applications.

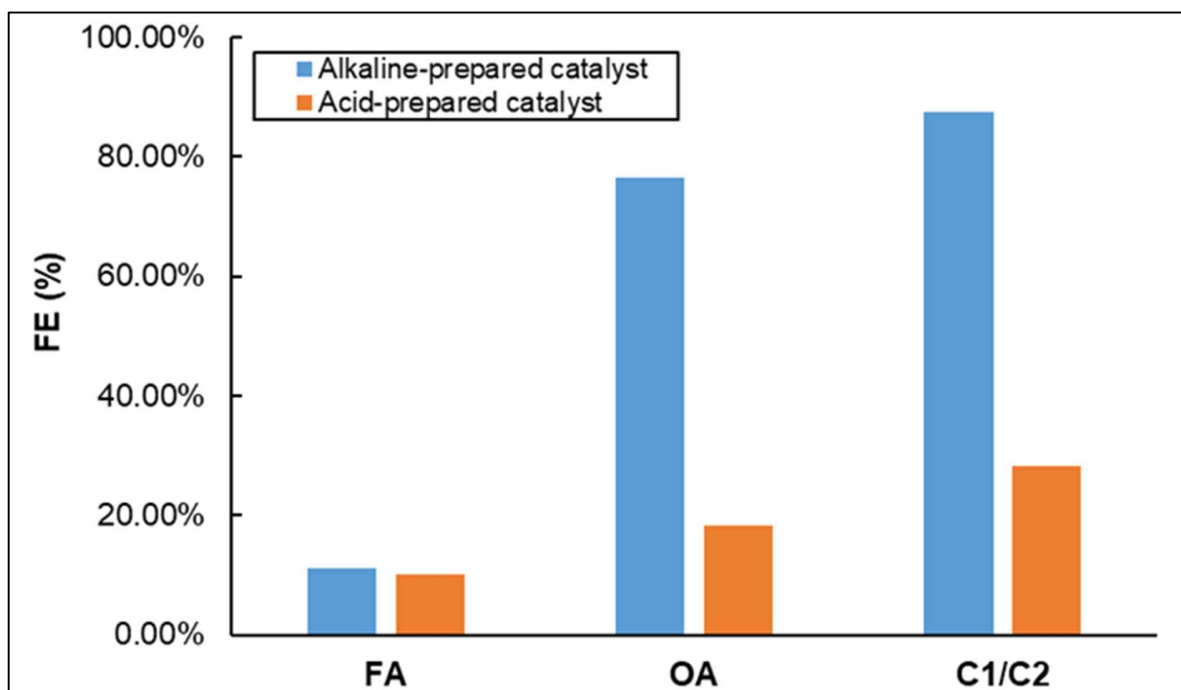


Fig. 10. Faradic efficiency (FE%) for formic acid (FA), oxalic acid (OA), and C1/C2 of eCO₂R using CuO/SnO₂ (1:1) NM prepared in alkaline and acid media. Experimental conditions: Anode: Pt (2cm²), Cathode: CuO/SnO₂@Ni foam (2 cm²), Electrolyte: 0.5 M KHCO₃, Separation membrane: Nafion 100, Applied voltage: - 1.4 V vs SCE, CO₂ flow rate: 10 mL/min, electrolysis duration: 3 hours.

3.3. Postmortem analysis of CuO/SnO₂ nanomaterials

Postmortem analysis was conducted to evaluate the structural and compositional changes in CuO/SnO₂ nanomaterials synthesized under acidic and alkaline conditions after prolonged electrochemical CO₂ reduction. The analysis utilized SEM, TEM, and XPS to assess morphological degradation, compositional stability, and surface modifications. These insights provide a deeper understanding of the catalysts' performance and durability.

3.3.1. SEM and SEM-EDS analysis

Post-reduction SEM images revealed distinct differences in the structural stability of nanomaterials synthesized under acidic and alkaline conditions (see Fig. 11). Alkaline-prepared samples retained their uniform particle distribution and spherical morphology, with no significant agglomeration observed (Fig. 11.a). The nanoparticles remained within the original size range (20–40 nm), indicating excellent structural integrity. In contrast, acidic-prepared samples exhibited severe particle agglomeration, surface roughness, and loss of morphological uniformity (Fig. 11.b). The particle size increased significantly (up to 80–120 nm), likely due to coalescence

and sintering during the reduction process. SEM-EDS analysis confirmed that alkaline-prepared samples maintained a consistent Cu/Sn atomic ratio close to 1:1 after reduction. However, acidic-prepared samples showed a notable decrease in Cu content, indicating leaching of Cu species during CO₂ reduction (Table 3). This loss of active sites contributed to the inferior catalytic performance and reduced durability of acidic-prepared nanomaterials.

Table 3. SEM/EDS element analysis of used CuO/SnO₂ NM prepared by sol-gel method in alkaline and acid media.

Elements	Alkaline medium		Acid medium	
	Elements at 2 μm (Atom %)	Elements at 200 nm (Atom %)	Element at 2 μm (Atom %)	Element at 200 μm (Atom %)
C	46.92	95.11	85.84	84.13
O	20.03	2.02	7.06	8.51
F	9.06	0.24	4.27	0.24
Al	0.32	0.03	0.04	0.13
Ni	0.75	0.01	0.13	0.30
Cu	13.69	1.22	0.07	0.22
Sn	8.86	1.08	2.57	5.69

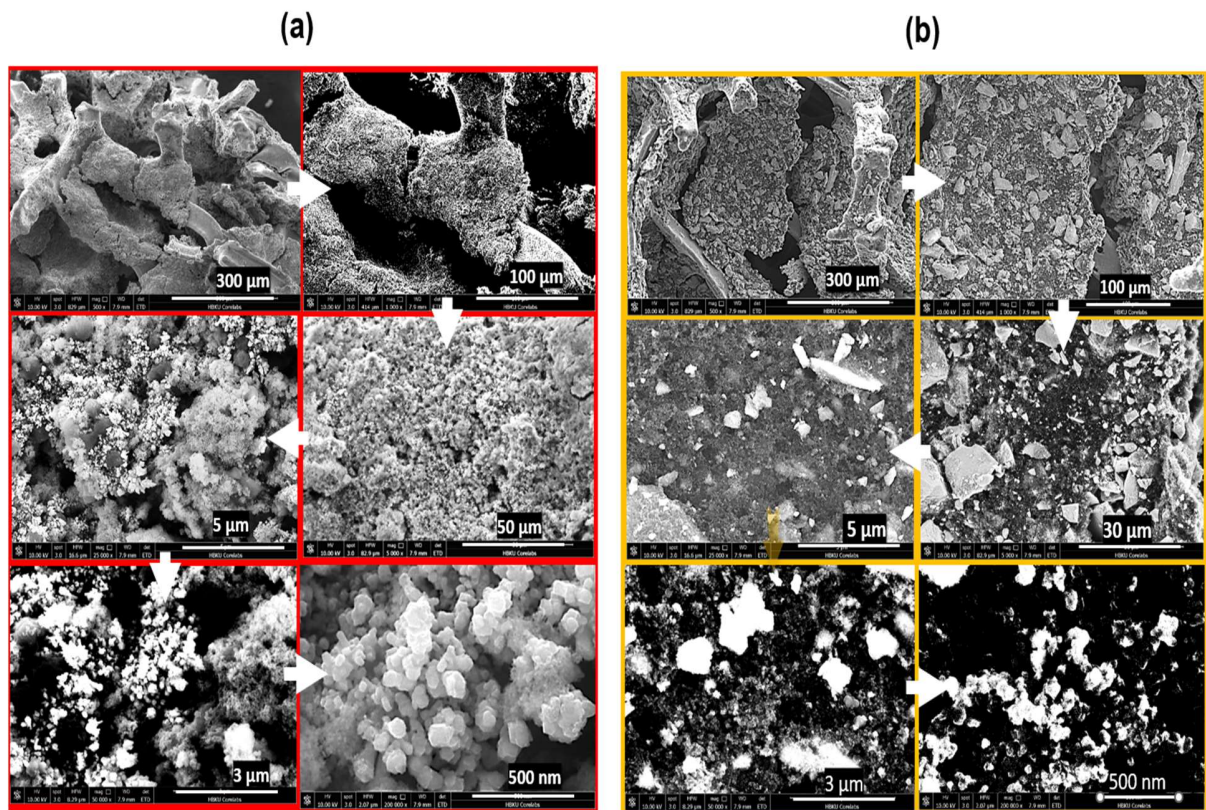


Fig. 11. Surface characterization by SEM within micro/nano scales after used of CuO/SnO₂ (1:1) NM prepared by sol-gel method in **a)** alkaline medium, and **b)** acid medium.

3.3.2. TEM and HRTEM analysis

TEM images of the alkaline-prepared samples showed minimal changes in nanoparticle size and shape after electrochemical reduction. High-resolution TEM (HRTEM) revealed that the lattice fringes corresponding to CuO (111) and SnO₂ (110) planes remained intact, confirming the preservation of crystallinity and phase composition (Fig.12.a). Electron diffraction patterns showed sharp rings, indicating that the crystalline structure of the nanomaterials was not compromised. In contrast, TEM images of acidic-prepared samples revealed significant structural degradation (Fig. 12.b). The nanoparticles lost their distinct boundaries and exhibited amorphous regions, indicating a partial collapse of the crystalline structure. The HRTEM images showed faint and discontinuous lattice fringes, corroborating the loss of crystallinity. Electron diffraction patterns displayed broader and less distinct rings, further confirming structural breakdown.

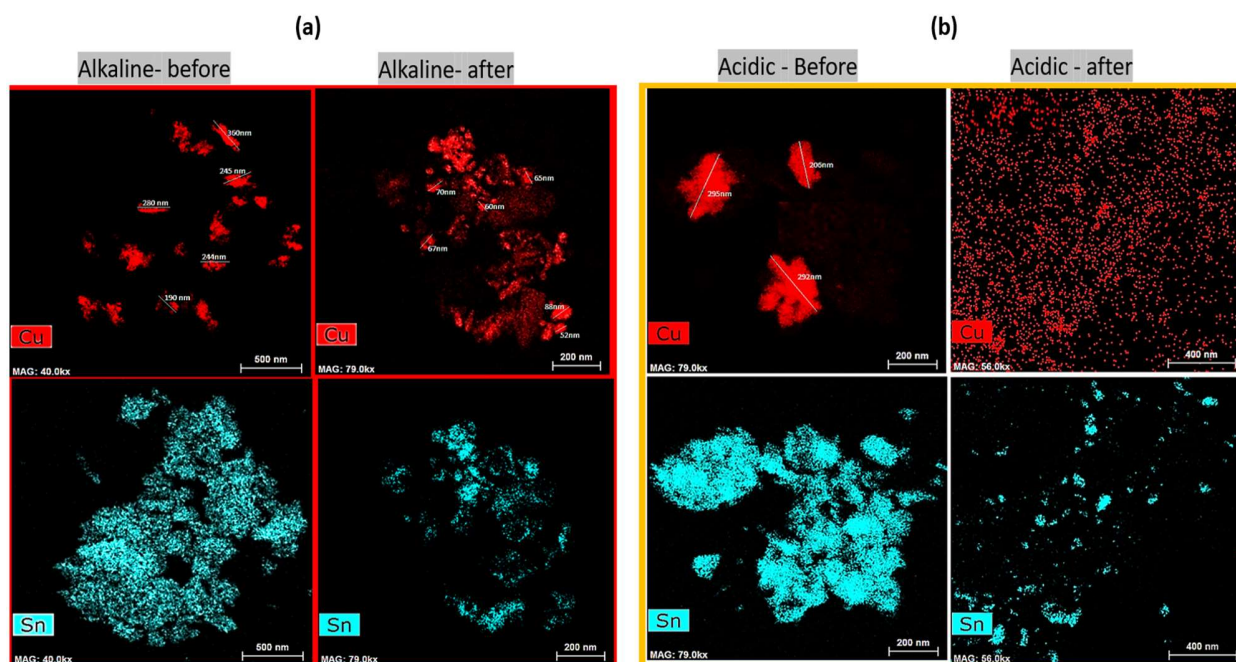


Fig. 12. TEM images of CuO/SnO₂ (1:1) NM prepared by sol-gel method **a)** alkaline medium, and **b)** acid medium, for monitoring of Cu and Sn before and after using in eCO₂R

3.3.3. XPS analysis

After electrochemical CO₂ reduction, significant differences emerged between the materials synthesized in alkaline and acidic media (Fig. 13 and 14). For alkaline-prepared samples, the Cu 2p spectrum displayed a shift in the Cu 2p_{3/2} peak to 932.5 eV and a decrease in the satellite peak intensity, indicating partial reduction of Cu²⁺ to Cu⁺ during the catalytic process (Fig. 13.a). This transformation highlights the active role of CuO in facilitating CO₂ reduction reactions. The Sn 3d spectrum remained largely unchanged, suggesting that SnO₂ retained its structural stability under the alkaline environment (Fig. 13.b). In the O 1s spectrum, an increase in the intensity of the hydroxyl peak (~532 eV) was observed, reflecting surface interactions with reaction intermediates (Fig. 14.a).

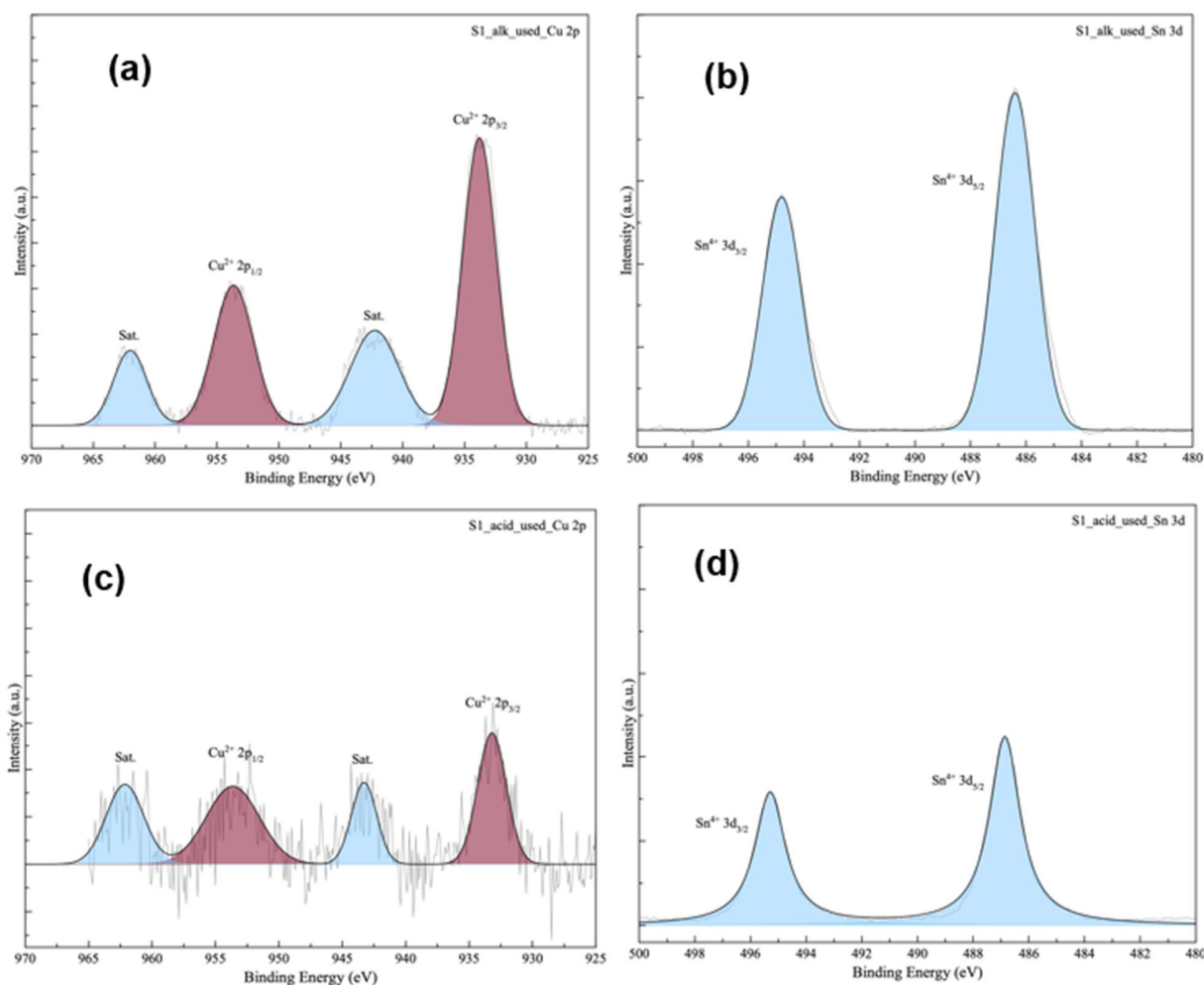


Fig. 13. XPS spectra of Cu 2p (a, c) and Sn 3d (b, d) of used CuO/SnO₂ NM samples prepared by sol-gel method in (a, b) alkaline medium, and (c, d) acid medium.

The C 1s spectrum showed a stronger signal for carbonate species at approximately 290.5 eV, confirming successful CO₂ adsorption and partial conversion into formic acid and other intermediates (Fig. 14.c). Conversely, the acidic-prepared nanomaterials exhibited significant structural degradation after electrochemical testing. The Cu 2p peaks showed a notable loss of intensity and increased broadening, indicating the leaching of Cu species and structural instability under acidic conditions (Fig. 13.b). The Sn 3d spectrum displayed minor shifts, suggesting partial instability of SnO₂, which further contributed to the reduced performance of these materials (Fig. 13.d). The O 1s spectrum showed an increase in adsorbed oxygen species, which corresponded to a decrease in lattice oxygen, highlighting surface defects and loss of structural integrity (Fig. 14.b). The C 1s spectrum also exhibited carbonate peaks, but with reduced intensity compared to alkaline-prepared materials, corroborating the lower catalytic activity and selectivity observed

during CO₂ reduction (Fig. 14.d). The partial reduction of Cu²⁺ to Cu⁺ in the alkaline samples highlights the role of copper in facilitating the catalytic process, while the stable SnO₂ phase provides structural support. The presence of carbonate species in the C 1s spectra further confirms effective CO₂ adsorption and conversion, particularly in alkaline-prepared materials. Overall, these findings underscore the significant influence of synthesis pH on the stability and catalytic activity of CuO/SnO₂ nanomaterials, with alkaline conditions yielding more robust and efficient electrocatalysts for CO₂ reduction.

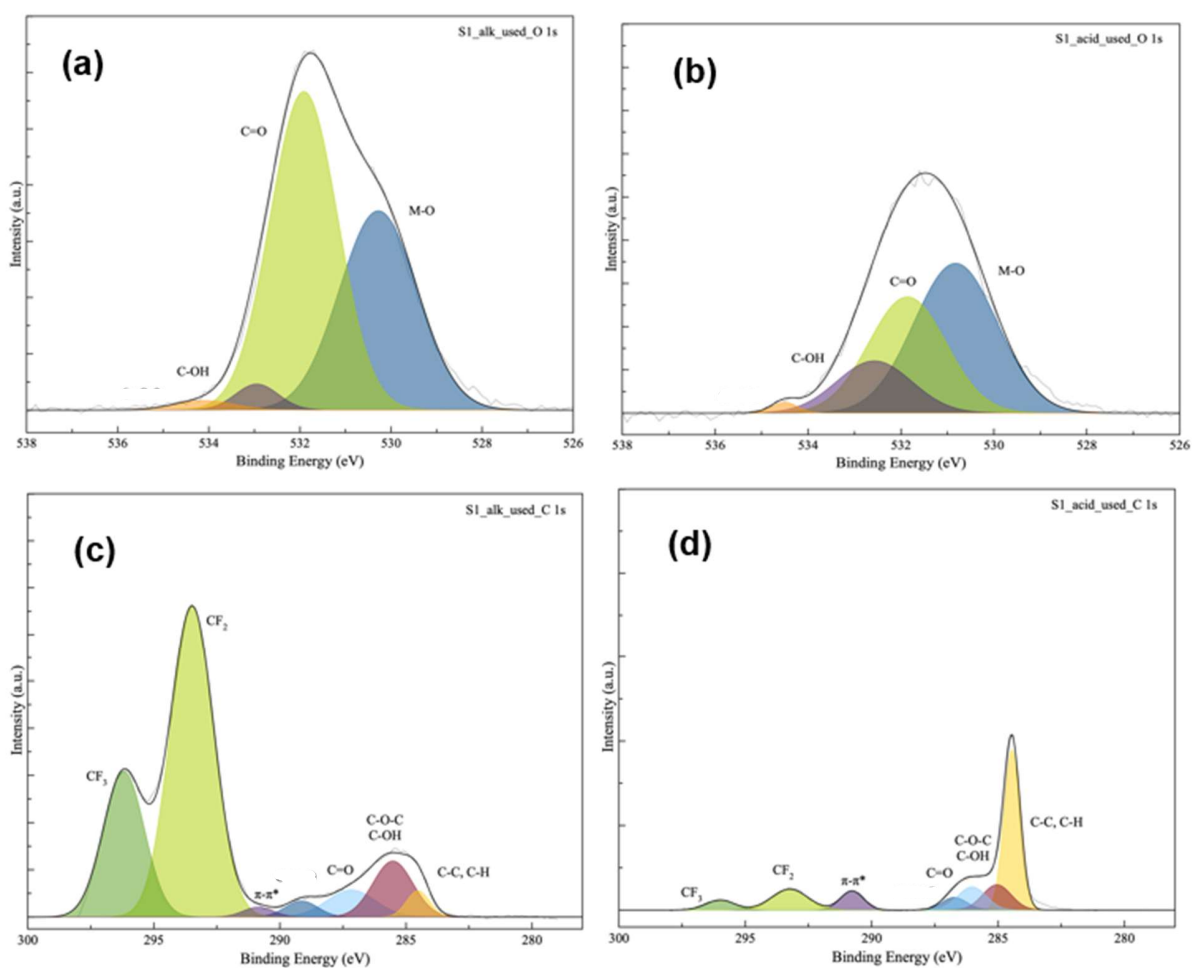


Fig. 14. XPS spectra of O 1s (a, b) and C 1s (c, d) of used CuO/SnO₂ NM samples prepared by sol-gel method in (a, c) alkaline medium, and (b, d) acid medium.

3.4. Stability and mechanistic insights

The alkaline-prepared CuO/SnO₂ nanomaterials maintained a stable current density and consistent Faradaic efficiency for C1/C2 throughout the experiment. Post-electrochemical characterization by SEM and XPS revealed minimal structural degradation or leaching of Cu and Sn components, confirming their robustness under operating conditions. In contrast, the acidic-

prepared samples exhibited significant performance degradation, with the current density decreasing by 40% over the same period. SEM images of the used acidic samples showed severe agglomeration and surface defects, while XPS analysis revealed leaching of Cu species and partial reduction of SnO₂. These structural changes account for the poor durability and reduced catalytic performance observed for acidic-synthesized materials. The superior performance of alkaline-prepared CuO/SnO₂ nanomaterials can be attributed to several factors. The high crystallinity and uniform particle distribution observed in alkaline samples provide a larger number of active sites for CO₂ adsorption and activation. The partial reduction of Cu²⁺ to Cu⁺, as confirmed by XPS, enhances the intermediate stabilization required for formic acid production. SnO₂ acts as a co-catalyst, facilitating proton transfer and stabilizing reaction intermediates, which together improve product selectivity and reduce side reactions. Acidic-prepared materials, despite exhibiting initial activity, suffer from lower crystallinity, poor structural integrity, and reduced stability under electrochemical conditions. These deficiencies lead to reduced active site availability and promote side reactions, thereby lowering the overall efficiency and selectivity of CO₂ reduction.

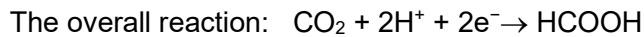
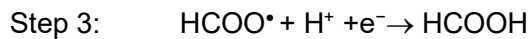
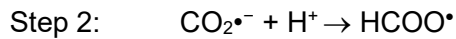
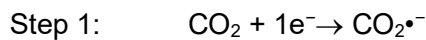
To address your concern about the long-term stability of the catalysts in different media, the experimental data from extended chronoamperometry tests. These tests were conducted for 12 hours under identical conditions for both alkaline- and acidic-prepared catalysts is summarized in table 4 to demonstrate that the alkaline-prepared CuO/SnO₂ nanomaterials retain over 90% of their initial performance, while the acidic-prepared catalysts exhibit significant degradation (up to 40% loss in current density). This comparison highlights the superior stability of alkaline-prepared materials, which we attribute to their higher crystallinity, structural integrity, and resistance to leaching.

Table 4: Total FE (%) for C1/C2 different electrolyte solution

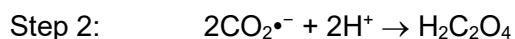
Total FE (%) for C1/C2		
Medium (electrolyte solution)	Alkaline-prepared CuO/SnO ₂	Acid -prepared CuO/SnO ₂
0.5 M K ₂ SO ₄	16.48%	
0.5 M KHCO ₃	87.60 %	28.33%
0.4 M K ₂ SO ₄	22.15%	10.12%
0.4 M KHCO ₃	63.65	29.47%
0.3 M K ₂ SO ₄	14.45	7.90%
0.3 M KHCO ₃	25.18	13.90%

The eCO₂R mechanisms to formic acid and oxalic acid involve multi-step proton-coupled electron transfer processes, with key differences arising at the intermediate and C–C coupling stages.

CuO/SnO₂ nanomaterials play a crucial role in facilitating these pathways by providing active sites for CO₂ activation and stabilizing reaction intermediates. The electrochemical reduction of CO₂ (eCO₂R) to formic acid (HCOOH) and oxalic acid (H₂C₂O₄) proceeds via a series of proton-coupled electron transfer steps, with the selectivity for each product determined by the catalyst properties, reaction conditions, and applied potential [47]. The process begins with the adsorption and activation of CO₂ molecules on the surface of CuO/SnO₂ nanomaterials. CO₂ adsorption is enhanced by oxygen vacancies on SnO₂ and partially reduced CuO sites. Adsorbed CO₂ is activated into a bent CO₂^{•-} radical anion, a crucial intermediate for both product pathways [48], [49], [50]. In the case of formic acid production, the CO₂^{•-} anion radical undergoes protonation and accepts another electron to form the carboxyl intermediate (*HCOO). This intermediate is stabilized by SnO₂, which facilitates proton transfer. A subsequent proton-coupled electron transfer step converts *HCOO into desorbed formic acid, completing the reduction. The overall reaction for formic acid production involves the transfer of two electrons and two protons to a single CO₂ molecule, generating HCOOH. CuO plays a critical role in stabilizing the electron transfer process, while SnO₂ enhances the efficiency of intermediate stabilization and proton transfer. The mechanism of formic acid production can be given by the following steps [51], [52].



For oxalic acid production, two adsorbed CO₂^{•-} radicals on adjacent active sites undergo a coupling reaction to form an oxalate intermediate (*C₂O₄²⁻). This step, which forms the C–C bond, is a key determinant of selectivity for C₂ products. CuO facilitates the multi-electron process required for C–C coupling, while SnO₂ supports intermediate stabilization through its oxygen vacancies. The oxalate intermediate is then desorbed as C₂O₄²⁻, completing the reaction. The overall process requires two electrons and two protons to produce a single oxalic acid molecule from two CO₂ molecules [47], [53].



The proposed mechanisms on the catalytic pathways for both formic acid (C1 product) and oxalic acid (C2 product) is illustrated in Fig. 15. Using insights from XPS analysis, the roles of CuO/SnO₂ in facilitating CO₂ adsorption, activation, and intermediate stabilization. Specifically, CuO

contributes to multi-electron transfer processes, while SnO₂ provides oxygen vacancies that stabilize intermediates such as CO₂^{•-} and facilitate proton transfer. A mechanistic schematic illustrates the pathways for CO₂ reduction to formic and oxalic acids, highlighting the key steps, active sites, and C–C coupling dynamics.

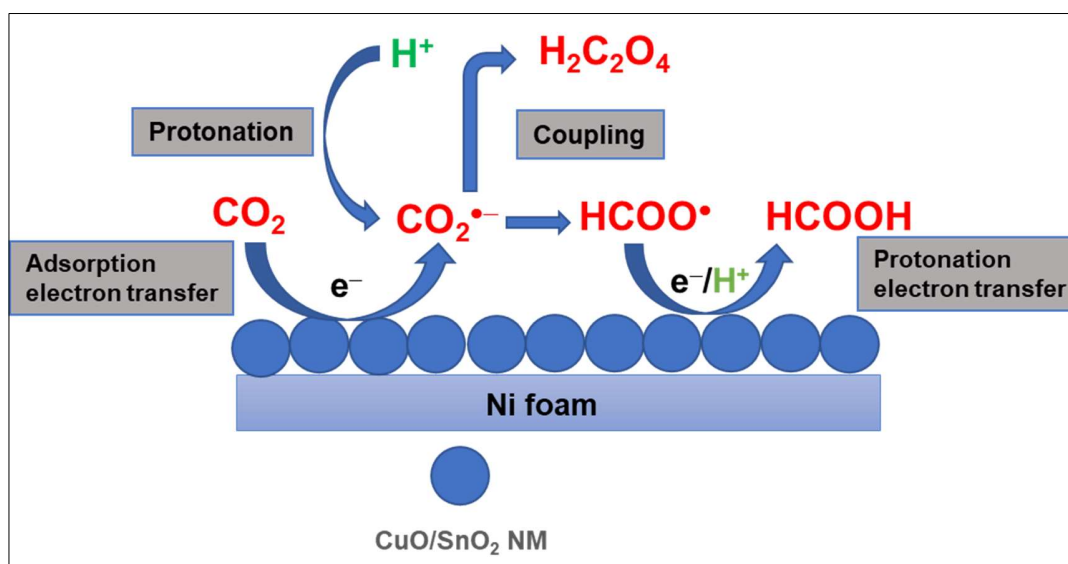


Fig. 15: The proposed mechanism of reaction for formic and oxalic acid formation using CuO/SnO₂ NM.

CuO and SnO₂ act synergistically to enable these pathways. CuO provides efficient electron transfer sites and stabilizes reaction intermediates, while SnO₂ enhances CO₂ adsorption and intermediate stabilization through its surface properties. Alkaline-prepared CuO/SnO₂ nanomaterials exhibit higher crystallinity and better-defined active sites, promoting oxalic acid formation as the dominant product. Formic acid production is typically favored at lower potentials where energy input is insufficient for C–C coupling. In contrast, higher potentials favor oxalic acid due to the energy requirements for C–C bond formation. Reaction conditions, including electrolyte pH and catalyst structure, also play a critical role. Alkaline conditions enhance intermediate stabilization, making them more favorable for oxalic acid production, while acidic conditions often lead to lower selectivity and efficiency due to competing side reactions and structural instability of the catalysts. The dual pathways for eCO₂R to formic and oxalic acids underscore the importance of tuning catalyst properties and reaction conditions to achieve the desired selectivity. CuO/SnO₂ nanomaterials provide an effective platform for both C1 and C2 product formation, with alkaline-prepared catalysts offering superior performance and stability. Further optimization of synthesis

and reaction parameters could enhance the efficiency and scalability of these materials for CO₂ reduction applications. Alkaline-prepared CuO/SnO₂ nanomaterials demonstrated superior overall Faradaic efficiency (87%) for C1/C2, higher current density, and better product selectivity compared to acidic-prepared samples. Faster electron transfer kinetics and improved structural stability under alkaline conditions significantly enhance catalytic performance. Acidic-prepared samples exhibited poorer durability due to particle agglomeration, leaching of Cu species, and structural degradation during prolonged operation. Mechanistic studies highlight the synergistic role of CuO and SnO₂ in promoting selective oxalic acid production, with alkaline-synthesized materials offering a distinct advantage. These findings emphasize the critical role of synthesis conditions in determining the performance of CuO/SnO₂ nanomaterials for electrochemical CO₂ reduction. Alkaline-prepared materials stand out as highly efficient and durable electrocatalysts, making them promising candidates for industrial-scale applications. Alkaline-prepared samples showed uniformly distributed nanoparticles with smaller sizes and less agglomeration compared to acidic-prepared samples. Elemental mapping confirmed the homogeneous distribution of Cu and Sn in alkaline-prepared samples, whereas acidic-prepared samples exhibited localized enrichment and Cu leaching after CO₂ reduction. TEM and HRTEM revealed better crystallinity, smaller particle sizes, and distinct lattice fringes for alkaline-prepared samples, contributing to their enhanced catalytic activity and stability. These results collectively highlight the critical role of synthesis pH in determining the morphology, composition, and structural integrity of CuO/SnO₂ nanomaterials. Alkaline-prepared samples exhibited superior properties, making them more effective and stable for CO₂ reduction.

4. Conclusions

In this study, CuO/SnO₂ (1:1) nanomaterials (NM) were synthesized using the sol-gel technique under both acidic and alkaline conditions to evaluate their structural properties and performance in electrochemical CO₂ reduction (eCO₂R). The comparative analysis between the two synthesis conditions highlights the critical influence of pH on the morphology, crystallinity, and stability of the prepared nanomaterials. Detailed characterization using XRD, SEM, TEM, XPS, and FTIR revealed that CuO/SnO₂ NM prepared in alkaline media exhibited smaller, more homogeneously distributed nanoparticles with enhanced surface stability compared to those synthesized in acidic media. The alkaline-prepared materials demonstrated reduced agglomeration, improved crystallite formation, and a more uniform Cu/Sn ratio, all of which contributed to superior catalytic performance. Electrochemical studies in a two-compartment cell, using CuO/SnO₂-coated Ni foam electrodes, showed that alkaline-prepared nanomaterials significantly outperformed their acidic counterparts. Under optimized conditions (-1.4 V applied voltage, 0.5 M KHCO₃ electrolyte,

and 3 hours of reaction time), the alkaline-prepared CuO/SnO₂ achieved an overall Faradaic efficiency (FE) of 87% for formic acid and oxalic acid production. In contrast, acidic-prepared nanomaterials exhibited reduced FE and lower formic acid yields, primarily due to structural instability and particle agglomeration. Post-electrochemical characterization of the used nanomaterials further confirmed the superior stability of alkaline-synthesized catalysts, with minimal degradation observed after prolonged operation. The results suggest that the enhanced activity and selectivity of CuO/SnO₂ NM synthesized in alkaline conditions arise from their larger surface area, higher structural uniformity, and improved electron transfer properties. Overall, this study demonstrates that tailoring the synthesis conditions, particularly pH, plays a vital role in optimizing the structural and electrochemical properties of CuO/SnO₂ nanomaterials. The sol-gel method, with its scalability and cost-effectiveness, provides a promising route for fabricating high-performance electrocatalysts for CO₂ reduction. Specifically, the ability to selectively produce formic acid with high efficiency highlights the potential of these materials for sustainable energy and chemical production.

Future research should focus on optimizing catalyst composition, exploring doping strategies, and investigating the effects of electrolyte pH and concentration to further enhance Faradaic efficiency, stability, and selectivity. Additionally, long-term operational studies and scaling-up processes will be essential to evaluate the practical applicability of these materials in industrial CO₂ reduction systems.

Conflicts of Interest

The authors declare no conflicts of interest.

Acknowledgements

The authors extend their gratitude to the Qatar National Research Fund (QNRF) for their support and provided via Grant # NPRP13S-0202-200228, and to the Qatar Shell Research Technology Center (QSRTC) as a co-founder, in addition authors would like to appreciate CORE lab in HBKU for their support in surface characterization.

References

- [1] Jie Zhang, Wen Luo, Andreas Züttel,, " Crossover of liquid products from electrochemical CO₂ reduction through gas diffusion electrode and anion exchange membrane," *Journal of Catalysis*, vol. 385, no. 202, pp. 140-145, 2020.
- [2] E.V. Kondratenko, G. Mul, J. Baltrusaitis, G.O. Larraz´abal, J. P´erez-Ramírez,, " , "Status and perspectives of CO₂ conversion into fuels and chemicals by catalytic, photocatalytic and electrocatalytic processes,, " *Energ. Environ. Sci.*, vol. 6, no. 11, 2013.
- [3] Liwei Jiang, Dejian Dong, and Yi-Chun Lu, , ""Design strategies for low temperature aqueous electrolytes," *Nano Research Energy*, vol. 1, no. 1, 2022.
- [4] Álvarez A, Borges M, Corral-Pérez JJ, Olcina JG, Hu L, Cornu D, Huang R, Stoian D, Urakawa A, , "CO₂ Activation over Catalytic Surfaces.," *Chemphyschem*, vol. 18, no. 22, pp. 3135-3141, 2017.
- [5] Mahinder Ramdin, Andrew R. T. Morrison, Mariette de Groen, Rien van Haperen,Robert de Kler, Leo J. P. van den Broeke, J. P. Martin Trusler, Wiebren de Jong,and Thijs J. H. Vlugt,, ""High Pressure Electrochemical Reduction of CO₂ to Formic Acid/Formate: A Comparison," *Industrial & Engineering Chemistry Research*, vol. 58, no. 5, pp. 1834-1847, 2019.
- [6] "Bui, Mai and Adjiman, Claire S. and Bardow, André and Anthony, Edward J. and Boston, Andy and Brown, Solomon and Fennell, Paul S. and Fuss, Sabine and Galindo, Amparo and Hackett, Leigh A. and Hallett, Jason P. and Herzog, Howard J. and Jackson, George a, "Carbon capture and storage (CCS): the way forward," *Energy Environ. Sci.*, vol. 11, no. 5, pp. 1062-1176, 2018.
- [7] Sodiq, Ahmed & Abdullatif, Yasser & Aïssa, Brahim & Ostovar, Arash & Nassar, Nashaat & El-Naas, Muftah & Amhamed, Abdukarem., "A review on progress made in direct air capture of CO₂," *Environmental Technology & Innovation*, vol. 29, no. 2, 2022.
- [8] Hasegawa, T., Fujimori, S., Ito, A. et al. , "Careful selection of forest types in afforestation can increase carbon sequestration by 25% without compromising sustainability," *Communications Earth & Environment*, vol. 5, no. 171, 2024.
- [9] Qi Lu a, Feng Jiao,, " "Electrochemical CO₂ reduction: Electrocatalyst, reaction mechanism, and process engineering," *Nano Energy*, pp. 439-456, 2016.

- [10] Fuping Pan, Huilei Zhao, Wei Deng, Ying Li,, " A novel N,Fe-Decorated carbon nanotube/carbon nanosheet architecture for efficient CO₂ reduction," *Nature Reviews Chemistry*, vol. 273, pp. 154-161, 2018.
- [11] Yuvraj Y. Birdja, Göttle, Federico Calle-Vallejo, Marc T. M. Koper, , " Advances and challenges in understanding the electrocatalytic conversion of carbon dioxide to fuels," *natural Energy*, vol. 04, pp. 732-745, 2019.
- [12] Mansoor Al-Shamari, Ahmed Khodary, Dong Suk Han, Iqbal M. Mujtaba, N. Rahmanian,, "Utilization of carbon dioxide using electrochemical reduction: A review,," *Gas Science and Engineering*,, vol. 127, p. 205367, 2024.
- [13] Bijandra Kumar, Baleeswaraiah Muchharla, Moumita Dikshit, Saudagar Dongare, Kapil Kumar, Burcu Gurkan, and Joshua M. Spurgeon, "Electrochemical CO₂ Conversion Commercialization Pathways: A Concise Review on Experimental Frontiers and Technoeconomic Analysis," *Environmental Science & Technology Letters*, vol. 11, no. 11, 2024.
- [14] Masood ul Hasan, Israr, et al.,, " Carbon-based metal-free catalysts for electrochemical CO₂ reduction: activity, selectivity, and stability," *Carbon Energy*, vol. 3, no. 1, pp. 24-49, 2021.
- [15] Qi Lu, Feng Jiao, " "Electrochemical CO₂ reduction: Electrocatalyst, reaction mechanism, and process engineering," *Nano Energy*, vol. 29, pp. 439-456, 2016.
- [16] Dazhong Zhong, Zhi-Jian Zhao, Qiang Zhao, Dongfang Cheng, Bin Liu, Wanyu Deng, Hao Dong, Lei Zhang, Jingkun Li, Jinping Li, Jinlong Gong,, " Coupling of Cu(100) and (110) Facets Promotes Carbon Dioxide Conversion to Hydrocarbons and Alcohols," *Angewandte Chemie*, vol. 60, no. 8, pp. 4870-4885, 2020.
- [17] Wanfeng Xiong, Duanhui Si, Jundong Yi, Yuanbiao Huang, Hongfang Li, Rong Cao, "Morphology and composition dependence of multicomponent Cu-based nanoreactor for tandem electrocatalysis CO₂ reduction," *Applied Catalysis B: Environmental*, vol. 60, no. 8, p. 121498, 2022.
- [18] Yangchun Lan, Gaoqiang Niu, Fei Wang, Dehu Cui, and Zhuofeng Hu. , "SnO₂-Modified Two-Dimensional CuO for Enhanced Electrochemical Reduction of CO₂ to C₂H₄. ACS Applied Materials & Interfaces," vol. 12, no. 32, pp. 36128-36136, 2020 .
- [19] M. Wang, H. Chen, M. Wang, J. Wang, Y. Tuo, W. Li, S. Zhou, L. Kong, G. Liu, L. Jiang, G. Wang,, " Tuning C₁/C₂ Selectivity of CO₂ Electrochemical Reduction over in-Situ Evolved CuO/SnO₂ Heterostructure.," *Angewandte Chemie International Edition*, 2023.
- [20] Xiao Chen, Dr. Yunxia Zhao, Jiayi Han, Prof. Yunfei Bu, "Copper-Based Catalysts for Electrochemical Reduction of Carbon Dioxide to Ethylene," *ChemPlusChem*, vol. 88, no. 1, 2023.
- [21] Bo Sun, Mingwei Dai, Songchi Cai, Haoyan Cheng, Kexing Song, Ying Yu, Hao Hu,, "Challenges and strategies towards copper-based catalysts for enhanced electrochemical CO₂ reduction to multi-carbon products,," *Fuel*, Vols. 332 - Part -1 , p. 126114, 2023.

- [22] Qiang Wang and Hehe Wei and Ping Liu and Zixiang Su and Xue-Qing Gong, "Recent advances in copper-based catalysts for electrocatalytic CO₂ reduction toward multi-carbon products," *Nano Research Energy*, vol. 3, p. 9120112, 2024.
- [23] Zhao, Jian and Xue, Song and Barber, James and Zhou, Yiwei and Meng, Jie and Ke, Xuebin, "An overview of Cu-based heterogeneous electrocatalysts for CO₂ reduction," *J. Mater. Chem. A*, vol. 8, no. 9, pp. 4700-4734, 2020.
- [24] Shulin Zhao, Sheng Li, Tao Guo, Shuaishuai Zhang, Jing Wang, Yuping Wu & Yuhui Chen, "Advances in Sn-Based Catalysts for Electrochemical CO₂ Reduction," *Nano-Micro Letters*, vol. 11, no. 1, 2019.
- [25] Mabrook S. Amer, Haneen A. AlOraij, Kuo-Wei Huang, Abdullah M. Al-Mayouf, "ray mesoporous SnO₂ catalyst for CO₂ electroreduction with high partial current density and formate selectivity," *Environmental Research*, Vols. 252, Part 2, p. 118897, 2024.
- [26] He, Yeheng and Jiang, Wen-Jie and Zhang, Yun and Huang, Lin-Bo and Hu, Jin-Song, "Pore-structure-directed CO₂ electroreduction to formate on SnO₂/C catalysts," *J. Mater. Chem. A*, vol. 7, no. 31, pp. 18428-18433, 2019.
- [27] Chunyue Shen, Ke Li, Yirui Ma, Shuang Liu, Xiaoyang Wang, Jingwen Xu, Mingming Wang, Yahan Meng, Na Chen, Wei Chen, "Electrochemical reduction of CO₂ via a CuO/SnO₂ heterojunction catalyst," *Chemical Physics Letters*, vol. 818, p. 140438, 2023.
- [28] Yang Yue, Xiaohuan Zou, Yuande Shi, Jiannan Cai, Yuxuan Xiang, Zhongshui Li, Shen Lin,, " A low crystallinity CuO-SnO₂/C catalyst for efficient electrocatalytic reduction of CO₂," *Journal of Electroanalytical Chemistry*, , vol. 928, p. 117089, 2023.
- [29] Kevin Fernández-Caso, Guillermo Díaz-Sainz, Manuel Alvarez-Guerra, and Angel Irabien., " Electroreduction of CO₂: Advances in the Continuous Production of Formic Acid and Formate.," *ACS Energy Letters*, vol. 8, no. 4, pp. 1992-2024, 2023 .
- [30] S. Varhade, A. Gururji, C. Singh, G. Cicero, M. García-Melchor, J. Helsen, D. Pant,, " Electrochemical CO₂ Reduction: Commercial Innovations and Prospects," *ChemElectroChem* , 2024.
- [31] Chunyue Shen, Ke Li, Yirui Ma, Shuang Liu, Xiaoyang Wang, Jingwen Xu, Mingming Wang, Yahan Meng, Na Chen, Wei Chen, , "Electrochemical reduction of CO₂ via a CuO/SnO₂ heterojunction catalyst.," *Chemical Physics Letters*, vol. 818, p. 140438, 2023.
- [32] Yang Yue, Xiaohuan Zou, Yuande Shi, Jiannan Cai, Yuxuan Xiang, Zhongshui Li, Shen Lin,, " A low crystallinity CuO-SnO₂/C catalyst for efficient electrocatalytic reduction of CO₂," *Journal of Electroanalytical Chemistry*,, vol. 298, p. 117089, 2023.
- [33] M. Fan, C. Ma, T. Lei, J. Jung, D. Guay and J. Qiao, " "Aqueous-phase electrochemical reduction of CO₂ based on SnO₂CuO nanocomposites with improved catalytic activity and selectivity.," *Catalysis Today*, vol. 2, no. 9, p. 318, 2018.

- [34] Maolin Zhang, Zedong Zhang, Zhenghang Zhao, Hao Huang, Dalaver H. Anjum, Dingsheng Wang, Jr-hau He, and Kuo-Wei Huang., "Tunable Selectivity for Electrochemical CO₂ Reduction by Bimetallic Cu–Sn Catalysts: Elucidating the Roles of Cu and Sn.," *ACS Catalysis*, vol. 11, no. 17, pp. 11103-11108, 2021.
- [35] RJayaseelan, MGopalakrishnan, "Synthesis and Characterization of Virgin and Ag doped CuO: SnO₂ Mixed Composites," *DJ Journal of Engineering Chemistry and Fuel*, vol. 2, no. 1, pp. 10-20, 2017.
- [36] Adeyemi, J.O.; Onwudiwe, D.C., "SnS₂ and SnO₂ Nanoparticles Obtained from Organotin(IV) Dithiocarbamate Complex and Their Photocatalytic Activities on Methylene Blue," *Materials*, vol. 13, no. 12, p. 2766, June 2020.
- [37] epideh Pazouki, Nafiseh Memarian, "Effects of Hydrothermal temperature on the physical properties and anomalous band gap behavior of ultrafine SnO₂ nanoparticles," *Optik*, vol. 246, p. 167843, 2021.
- [38] Sunny Kumar, S. Suresh, "Study of photodegradation and wetting behavior on synthesis oxides of tin (stannous and stannic),," *Materialia*, vol. 14, p. 100869, December 2020.
- [39] S. Amuthameena, K. Dhayalini, B. Balraj, C. Siva, N. Senthilkumar, "Two step synthesis and electrochemical behavior of SnO₂ nanomaterials for electrical energy storage devices,," *Inorganic Chemistry Communications*, vol. 131, September 2021.
- [40] Sudha Periathai, R., Pon Vengatesh, R., Abarna, S. et al, "Treatment of water pollution system using SnO₂ nanoparticles synthesized by sol–gel process," *Applied Nanoscience*, vol. 14, no. 1, pp. 135-147, october 2023.
- [41] V. Perumal, R. Uthrakumar, M. Chinnathambi, C. Inmozhi, R. Robert, M.E. Rajasaravanan, A. Raja, K. Kaviyarasu, "Electron-hole recombination effect of SnO₂ – CuO nanocomposite for improving methylene blue photocatalytic activity in wastewater treatment under visible light," *Journal of King Saud University - Science*, vol. 35, no. 1, p. 102388, january 2023.
- [42] Jorge Alejandro Torres-Ochoa, Dagoberto Cabrera-German, Orlando Cortazar-Martinez, Mariela Bravo-Sanchez, Gustavo Gomez-Sosa, Alberto Herrera-Gomez, "Peak-fitting of Cu 2p photoemission spectra in Cu₀, Cu¹⁺, and Cu²⁺ oxides: A method for discriminating Cu₀ from Cu¹⁺,," *Applied Surface Science*, vol. 622, p. 156960, 2023.
- [43] Jorge Alejandro Torres-Ochoa, Dagoberto Cabrera-German, Orlando Cortazar-Martinez, Mariela Bravo-Sanchez, Gustavo Gomez-Sosa, Alberto Herrera-Gomez, " Peak-fitting of Cu 2p photoemission spectra in Cu₀, Cu¹⁺, and Cu²⁺ oxides: A method for discriminating Cu₀," *Applied surface science* , vol. 622, p. 156960, 2023.
- [44] Hicham Idriss, " On the wrong assignment of the XPS O1s signal at 531–532 eV attributed to oxygen vacancies in photo- and electro-catalysts for water splitting and other materials," *applications, Surface Science*, vol. 712, p. 121894, 2021.

- [45] Matthew Smith, Louis Scudiero, Juan Espinal, Jean-Sabin McEwen, Manuel Garcia-Perez, , "Improving the deconvolution and interpretation of XPS spectra from chars by ab initio calculations, ,, " *Carbon*, vol. Volume 110, pp. 155-171, 2016.
- [46] Angga Hermawan, Yusuke Asakura, Miki Inada, Shu Yin, "A facile method for preparation of uniformly decorated-spherical SnO₂ by CuO nanoparticles for highly responsive toluene detection at high temperatur," *Journal of Materials Science & Technology*, vol. 51, pp. 119-129, August 2020.
- [47] Vera Boor, Jeannine E. B. M. Frijns, Elena Perez-Gallent, Erwin Giling, Antero T. Laitinen, Earl L. V. Goetheer, Leo J. P. van den Broeke, Ruud Kortlever, Wiebren de Jong, Othonas A. Moulton, Thijs J. H. Vlugt, and Mahinder Ramdin., "Electrochemical Reduction of CO₂ to Oxalic Acid: Experiments, Process Modeling, and Economics," *Industrial & Engineering Chemical Research* , vol. 61, no. 40, pp. 14837-14746, 2022.
- [48] Gennaro, A.; Isse, A. A.; Severin, M.-G.; Vianello, E.; Bhugun, I.; Savéant, J.-M, ". Mechanism of the electrochemical reduction of carbon dioxide at inert electrodes in media of low proton availability. ., 1996, 92, 3963– 3968," *J. Chem. Soc Faraday Trans. 1*, vol. 92, pp. 3963-3968, 1996.
- [49] Ikeda, S.; Takagi, T.; Ito, K. , "Selective Formation of Formic Acid, Oxalic Acid, and Carbon Monoxide by Electrochemical Reduction of Carbon Dioxide," *Bulletin of the Chemical Society of Japan*,, vol. 60, no. 7, p. 2517–252, 1987.
- [50] Subramanian, S.; Athira, K.; Anbu Kulandainathan, M.; Senthil Kumar, S.; Barik, R., " New insights into the electrochemical conversion of CO₂ to oxalate at stainless steel 304L cathode.," *J. CO₂ Util*, vol. 36, pp. 105-115, 2020.
- [51] Löwe, A.; Schmidt, M.; Bienen, F.; Kopljar, D.; Wagner, N.; Klemm, E, ". Optimizing Reaction Conditions and Gas Diffusion Electrodes Applied in the CO₂ Reduction Reaction to Formate to Reach Current Densities up to 1.8 A cm⁻²," *ACS Sustain. Chem. Eng.* , vol. 9, pp. 4213-4223, 2021.
- [52] Wang, Y.; Zhang, N.; Huang, C.; Xu, T., " Production of monoprotic, diprotic, and triprotic organic acids by using electrodialysis with bipolar membranes: Effect of cell configurations," *Journal of Membrane Science*,, vol. 385–386, pp. 226-233, 2011.
- [53] M. Marx, H. Frauendorf, A. Spannenberg, H. Neumann and M. Beller, "Revisiting Reduction of CO₂ to Oxalate with First-Row Transition Metals: Irreproducibility, Ambiguous Analysis, and Conflicting Reactivity," *JACS AU*, vol. 2, no. 3, p. 731– 744, 2022.